https://doi.org/10.5194/egusphere-2026-1496
Preprint. Discussion started: 20 March 2026

Seasonal variation in vegetation-climate interactions shape the CO_2 exchange in a degraded raised bog

Nicolas Behrens[1], Klaus-Holger Knorr[2], Christoph Rückriem[3], Mana Gharun[1]

[1]University Münster, Institute of Landscape Ecology, Biosphere Atmosphere Interaction, Münster, Germany
[2]University Münster, Institute of Landscape Ecology, Ecohydrology and Biogeochemistry, Münster Germany
[3] Biological Station Zwillbrock e.V., Vreden, Germany

Correspondence to: Nicolas Behrens (nicolas.behrens@uni-muenster.de)

Abstract.

Pristine peatlands act as natural carbon sinks, but disturbance — mostly anthropogenic drainage — turns them into CO_2 sources, responsible for 2–5% of annual greenhouse gas (GHG) emissions globally. Complex interactions between vegetation, soil, climate, and hydrology produce highly variable CO_2 budgets on different types of peatlands and between years. Abandoned drained peatlands are considered low-hanging fruit for rewetting due to expected high GHG emissions and low resistance to repurposing yet remain underrepresented in research. To close this gap in literature we measured three years (2023–2025) of CO_2 and CH_4 fluxes alongside meteorological and hydrological conditions in a drained shrub-dominated ombrotrophic raised bog in NW Germany, investigating carbon flux budgets and the main seasonal drivers of fluxes. Methane fluxes were negligible throughout, likely due to consistently deep water tables (>15 cm). Annual CO_2 budgets were highly variable: the site was a considerable source in 2023 and 2025 (131 and 86 gC m^{-2} a^{-1}) but near-neutral in 2024. An anomalously warm spring in 2024 triggered earlier vegetation greening and substantially increased CO_2 uptake capacity from April through June. In contrast, warming later in the growing season increased CO_2 emissions due to a stronger reaction of respiration than of photosynthesis to warming — highlighting how the timing of climate anomalies matters. Partitioning the effects of high air temperature (TA) and vapor pressure deficit (VPD) revealed that high VPD suppressed carbon fluxes in the first half of the growing season but not the second, while extreme TA did not limit GPP or ecosystem respiration the way extreme VPD did. TA and solar radiation were the dominant daily flux drivers; water table depth did not govern daily or interannual carbon flux variability. Together, our results demonstrate that the timing of TA and VPD anomalies — mediated through vegetation responses — decisively shapes their impact on the carbon balance. These results will become increasingly relevant as climate extremes intensify with ongoing global warming.

https://doi.org/10.5194/egusphere-2026-1496
Preprint. Discussion started: 20 March 2026

1 Introduction

Peatlands cover only 3% of the Earth's land surface, but they are the largest terrestrial carbon storage with about 30% of the global soil carbon, equivalent to an estimated 600 GtC (Yu et al., 2010). Pristine peatlands are waterlogged and the resulting anoxic conditions limit microbial decomposition of the peat through thermodynamic, enzymatic, and transport related constraints (Limpens et al., 2008). Peat forming vegetation takes up CO_2 through photosynthesis and due to slow and incomplete decomposition this carbon is stored as peat over millennia, turning natural peatlands into net carbon sinks. However, drainage of peatlands for peat extraction, forestry, or agriculture (Leifeld & Menichetti, 2018) leads to the aeration of the peat column, easing the constraints on microbial decomposition, leading to carbon losses in form of CO_2. The resulting emissions are estimated to account for 2-5% of annual anthropogenic greenhouse gas (GHG) emissions (Humpenöder et al., 2020; Leifeld & Menichetti, 2018; Ma et al., 2022), in countries with a large percentage of degraded peatlands such as Germany even up to 7% (Umweltbundesamt, 2022), making it an integral part of the anthropogenic carbon footprint.

Carbon fluxes from peatlands are governed by a complex interplay of components, including microbial communities (Mäkiranta et al., 2009), enzyme activities (Pinsonneault et al., 2016), thermodynamic limitations (Blodau, 2011), peat quality (Nielsen et al., 2023) and both vegetation composition and their phenological cycle (Korrensalo et al., 2020; Peichl et al., 2018), all of which interact with changing climatic and hydrological conditions across years (Adkinson et al., 2011; Alekseychik et al., 2021; Drollinger et al., 2019; Olson et al., 2013). This complexity results in a high variability in carbon fluxes between different peatlands and across years with contrasting climatic or hydrological conditions. Given their crucial role in the carbon cycle, it is essential to accurately represent peatlands in landscape management and upscaling models. This in turn requires a robust understanding of the underlying drivers for the heterogeneous range of peatland ecosystems and under variable climatic conditions. While several studies have quantified carbon balances and derived driving mechanisms at actively managed sites (H. He & Roulet, 2023; Tiemeyer et al., 2016) or following rewetting interventions (Kalhori et al., 2024; Nugent et al., 2018; Satriawan et al., 2023), drained and unutilized peatlands remain a gap in the current literature. They represent the in-between state when active management has ceased but no restoration measures are yet in place. Such sites are not yet represented in the IPCC guidelines for emissions from wetlands (IPCC, 2014), and while they are included in the German national emission factors (Tiemeyer et al., 2020), the wide uncertainty interval of emissions (0.7 to 10.8 tC ha^{-1} yr^{-1}) reflects the heterogeneity of carbon fluxes at sites in this category. The potentially substantial emissions due to the disturbance and relatively low resistance regarding the repurposing of such sites, in comparison for example to actively managed agricultural areas, make abandoned drained peatlands a low hanging fruit for climate mitigation measures (Guo et al., 2025).

https://doi.org/10.5194/egusphere-2026-1496
Preprint. Discussion started: 20 March 2026

The intensity of the drainage, often expressed through the average annual water table depth (WTD), is widely considered to be the most important driver of annual CO_2 emissions and was repeatedly used to infer CO_2 budgets across peatlands and peatland types based on functional relationships of GHG-fluxes to WTD (Evans et al., 2021; Koch et al., 2023; Tiemeyer et al., 2020). Site-scale studies repeatedly showed that increased WTD decisively controls net CO_2 emissions (Aslan-Sungur et al., 2016; Drollinger et al., 2019; Laine et al., 2019; Q. Li et al., 2021; Satriawan et al., 2023). This control is mostly attributed to increased ecosystem respiration (Reco) due to a deeper aeration of the peat column and higher microbial activity with rising air temperatures (TA) (Aslan-Sungur et al., 2016; Drollinger et al., 2019; Wilson et al., 2016). Additionally, with increasing WTD peat respiration can become more sensitive to rising TA (Denager et al., 2026; Liu et al., 2024), creating a feedback between warming and drying. However, the relationship between WTD fluctuations and Reco can break down when WTD is consistently high (> 20 cm), due to a limited response of pore space water saturation to further changes in WTD and decreasing peat quality with depth (Lafleur, Moore, et al., 2005; Waddington et al., 2001). Microbial respiration may be directly limited through moisture constraints (Estop-Aragonés & Blodau, 2012; Mäkiranta et al., 2009). Further, a high relative contribution of autotrophic respiration to Reco, which can make up 50% to 70% in shrub- or sedge-dominated peatlands (Rankin 2022, 2023), can lead to a reduced sensitivity of CO_2 emissions to WTD fluctuations (Juszczak et al., 2013; Lafleur, Moore, et al., 2005). As abandoned extraction sites and drained, degraded sites in many cases exhibit consistently deep WTD and a predominance of rushes, shrubs and sedges, the inference of CO_2 budgets based on simple transfer functions relying on singular predictors such as WTD may lead to erroneous estimates and requires a more detailed analysis of underlying driving factors of CO_2 budgets.

Besides the varying respiration rates, changes in net CO_2 exchange are potentially driven by the variability in gross primary production (GPP) through interannual differences in phenology, TA, and incoming radiation (Drollinger et al., 2019; Järveoja et al., 2018; Peichl et al., 2018). Both the magnitude and the timing of climate anomalies may change phenological development, either enhancing or decreasing net CO_2 uptake (Helbig et al., 2022; Helfter et al., 2015; Peichl et al., 2014). The light use efficiency, meaning the amount of carbon uptake per light received, correlates in peatlands with warmer TA and water availability, varying in strength with vegetation composition (Kross et al., 2016). Hot TA along with increased atmospheric dryness, expressed as vapor pressure deficit (VPD), may reduce GPP through a stomatal regulation feedback, employed to regulate water loss (Grossiord et al., 2020). While a large-scale analysis suggests that TA-driven increases in VPD do not substantially constrain biomass growth across northern peatlands (N. Chen et al., 2023), site-level studies on peatlands repeatedly report reductions in midday ecosystem CO_2 uptake under high VPD (Aurela et al., 2007; Goodrich et al., 2015; Humphreys et al., 2006; Poczta et al., 2023). The magnitude of this response varies with vegetation composition: graminoids and sedges may exhibit a stronger stomatal sensitivity to high VPD than shrubs (Gobin et al., 2015), even independent of groundwater availability (Goodrich et al., 2015; Otieno et al., 2012; Speranskaya et al., 2024).

https://doi.org/10.5194/egusphere-2026-1496
Preprint. Discussion started: 20 March 2026

To understand what drives carbon fluxes from abandoned drained bogs and to delineate the mitigation potential of restoration measures under a warming climate demands both precise flux measurements and a rigorous analysis of their drivers. Yet the magnitude of carbon fluxes in abandoned, drained peatlands, and how they respond to interacting climatic and environmental pressures, remains poorly understood. This study addresses that gap through three objectives: 1) quantifying monthly and annual CO_2 and CH_4 dynamics to establish net carbon budgets for a drained and shrub-dominated raised bog across three years (2023–2025); 2) determining how climate and hydrology — air temperature, water table depth, vapour pressure deficit, and radiation — govern carbon fluxes under both normal and extreme conditions; and 3) disentangling the impact of climatic anomalies temporally, revealing how the timing of their occurrence shapes carbon fluxes and ecophysiological responses.

Using continuous measurements of CO_2 and CH_4 fluxes collected with the eddy covariance method, we quantify the relationships between ecosystem carbon exchange and key climate drivers. Seasonal transitions are identified to delineate phenological phases. We identify the main climatic drivers of carbon flux variability using anomaly regression analysis. Ecophysiological response functions are used to derive ecosystem functional parameters, including the temperature sensitivity of Reco (Q_{10}) and the maximum photosynthetic uptake capacity (P_{max}). Changes in these parameters are then used to assess potential shifts in the ecosystem–climate feedback. Finally, the effects of high TA and VPD on ecosystem carbon fluxes are evaluated across different stages of the growing season by isolating their respective influences using a targeted filtering procedure.

Methods

2.1 Site description

The study site is located within the Amtsvenn-Hündfelder Moor. It is a degraded raised bog of roughly 600 ha on the German Dutch border between Gronau and Ahaus, in the state of North Rhine-Westphalia in Germany (Fig. 1). The EC tower at the site (DE-Amv) is an ICOS (Integrated Carbon Observation System) associate station implementing high quality standardized greenhouse gas flux observations (Gharun & Behrens, 2025).

In this degraded raised bog, peat cutting stopped in 1979, but drainage ditches remained largely open. Peat thickness (predominantly *Sphagnum* peat) at the site is roughly 4.3 m, with the upper 10-25 cm of peat being affected from degradation due to drainage, as reflected in lower C to N ratios (30-40), elevated N (1.5-2.0 %) and P (500-800 mg kg^{-1}) content and increased degree of peat decomposition compared to the underlying pristine peat (Lemmens et al., 2026). In the investigated area the peat body was mostly not cut except for the outermost margins. Water is continuously lost from the raised peat block to the adjacent lower parts of the bog where peat extraction took place and through an open drainage ditch to the south of the site. A vegetation survey on five sampling points within the footprint was conducted in July 2022. Vegetation consists to the largest degree of dwarf shrubs with a coverage of 50% to 75% *Calluna vulgaris,* 25% to 50%

https://doi.org/10.5194/egusphere-2026-1496
Preprint. Discussion started: 20 March 2026

Erica tetralix and individuals of *Vaccinium oxycoccos* and *Andromeda Polifolia*. Interspersed are patches of graminoids, mostly *Molinia caerulea,* with a cover of up to 25% and higher coverage at the outer margins of the investigated area. Along overgrown drainage ditches individuals of birches (both *Betula pubescens* and *Betula pendula*) grow, with smaller individuals scattered in the footprint (Fig. 1). Typical peatland (*Sphagnum* spp.) mosses are barely present any more, only a few individuals can be found in drainage ditches and outside of the tower footprint in low lying ponds. To control the encroachment of the woody vegetation the site is managed with light sheep grazing.

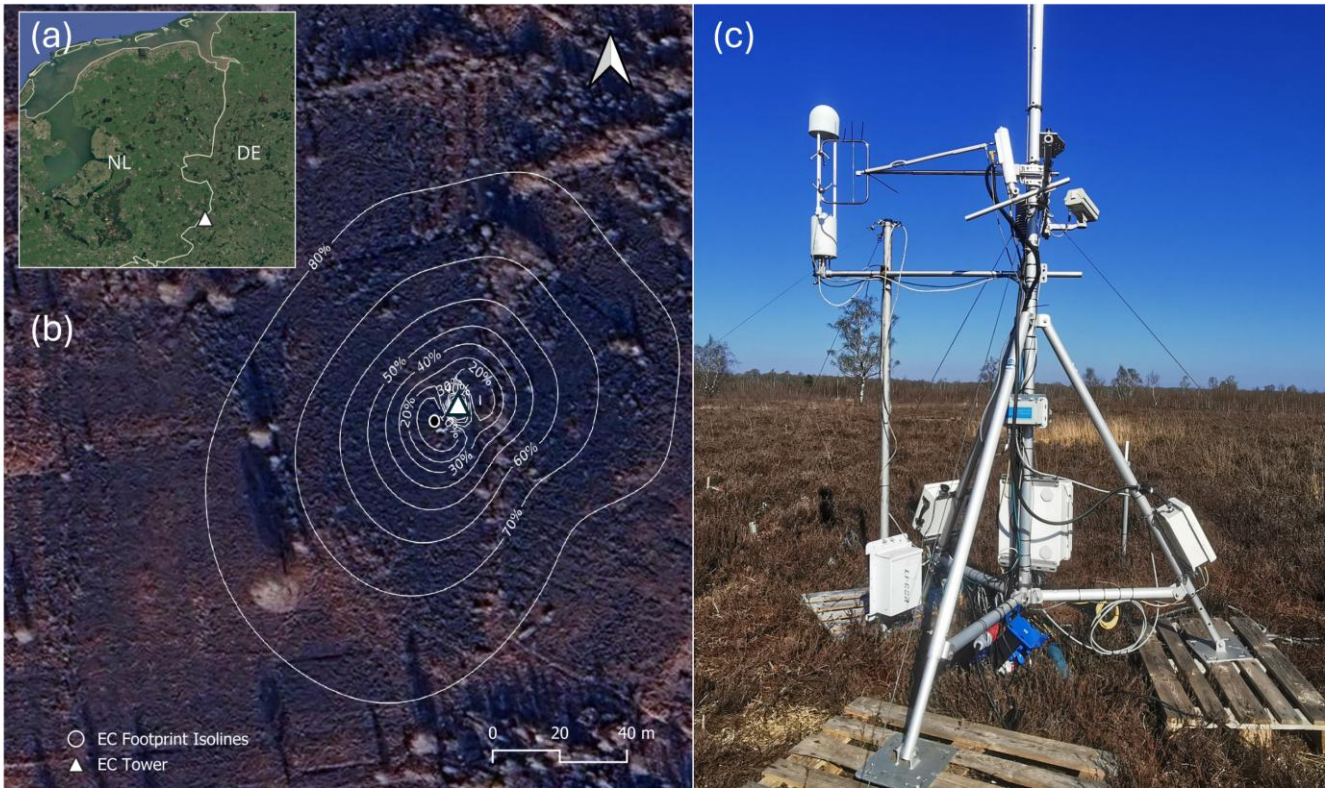

Figure 1: (a) shows the location of the measurement site on the border between Germany and the Netherlands. The white lines in (b) are the isolines of gas flux contribution from the footprint of the eddy covariance (EC) tower. (c) shows the setup of the tower with its surrounding ericaceous vegetation as well as some individual *Betula* trees and a patch of *Molinia caerulea* in the background. Background on the left side: Imagery © 2025 NASA, Map data © 2025 Google

2.2 Meteorological measurements

Several ancillary climatic and edaphic variables were recorded at a frequency of one minute and aggregated to half-hourly means. TA and relative humidity (RH) were measured with a Vaisala HMP 155. Precipitation (P) was measured with a non-heated rain gauge Texas Instruments 55202. Four radiation components consisting of upward (SWOUT) and downward (SWIN) shortwave and longwave (LWOUT and LWIN) radiation were measured with a heated Kipp & Zonen CNR4 net

https://doi.org/10.5194/egusphere-2026-1496
Preprint. Discussion started: 20 March 2026

radiometer. Soil variables were measured in two soil profiles, each at 5 cm depth. Soil water content (SWC) and soil temperature (TS) were measured with Stevens Hydraprobe II, secondary measurements of TS were conducted with LI-COR 7900-180 TS sensors. Soil heat flux (SHF) was measured with self-calibrating Hukseflux HFP01SC plates at 5 cm depth.

All meteorological data was screened for faulty measurements. In a first step the resulting gaps were filled from a secondary meteorological tower 20 m from the EC tower, which provided measurements of TA, RH, P and SWC (with sensors in that order being: S-THB-M00x, S-RGB-M002, S-SMC-M005, all by Onset Hobo, Bourne, MA, USA). Remaining gaps in TA, RH and P were filled with data from the station Ahaus of the german meteorological weather service DWD (station ID: 7374), ca. 10 km from the station. Potential offsets between the data sources due to different sensors or measurement heights or depths were corrected using ordinary least squares regression (OLS). Global radiation was not available from any auxiliary tower, so final remaining gaps in SWIN were closed using machine learning, specifically with the XGBoost regression tree method (T. Chen & Guestrin, 2016), using the day-of-year, the hour of the day, TA, P and SWIN derived from the ERA5land (Muñoz-Sabater et al., 2021) dataset as predictors.

The water table depth was measured by a pressure transducer ca. 20 meters from the tower (MX2001 connected to a RX3000 data logger, Onset Hobo, Bourne, MA, USA). A second WTD logger was installed ca. 50 m from the tower as part of the Moorbodenmonitoring (MoMoK) project by the Thünen Institute of Climate-Smart Agriculture (Frank et al., 2025). The first WTD logger had several power outages and was moved in the beginning of 2025, resulting in data gaps. The logger installed by the Thünen-Institute covered the full period from 19.09.2023 until 05.03.2025. To create a full time series spanning from beginning of 2023 until the end of 2025 the two data sources were combined with an ordinary least squares (OLS) regression between them to correct potential linear offsets ($R^2 = 0.91$).

2.3 Eddy covariance measurements and flux data processing

An eddy covariance (EC) tower was installed in September 2022. The tower setup includes a LI7200RS closed path infrared gas analyzer (LI-COR Inc., Lincoln, Nebraska, USA) and a Gill HS-50 (Gill Instruments Ltd., Lymington, Hampshire, UK) anemometer. In December 2023 an LI7700 open path CH_4 analyser (LI-COR Inc., Lincoln, Nebraska, USA) was added to the setup. The fluxes are measured on a tripod at 2.77 m height and with a frequency of 10 Hz. The raw EC data was processed into half-hourly aggregates using the EddyPro software version 7 by LI-COR and adhering to best practices agreed on by the community (Sabbatini et al., 2018). Raw 10 Hz data was filtered for spikes, dropouts and absolute limits (Vickers & Mahrt, 1997). Anemometer tilt was corrected using the double-rotation method (Wilczak et al., 2001). Time-lags between measurements of gas concentrations and wind components were accounted for using the covariance maximization method (Fan et al., 1990). Spectral losses were corrected by deriving reference (co)spectra for well-developed turbulent conditions and then correcting measurement spectra for high-pass and low-pass filtering effects (Fratini et al., 2012; Moncrieff et al., 2005). CH_4 fluxes measured with the open-path analyser were corrected for density fluctuation using the WPL correction (Webb et al., 1980).

https://doi.org/10.5194/egusphere-2026-1496
Preprint. Discussion started: 20 March 2026

The processed half-hourly fluxes were filtered to remove outliers, periods with erratic behaviour potentially induced by faulty sensors and poorly developed turbulent conditions. As a first step all data points with a quality flag of 2 were removed from the dataset, following the quality flagging system with flags 0, 1 and 2 (Mauder & Foken, 2011). To remove outliers representing unrealistically high fluxes we determined the 99.9% and 0.1% quantiles of the highest quality fluxes (flag 0 based on the flags mentioned above) separately for day and night-time of CO_2, CH_4, the sensible heat flux H and the latent heat flux LE. Values above and below these thresholds were removed. Nightly conditions were determined using a threshold of less than 10 W/m^2 SWIN. After the absolute limits removal remaining spikes were determined with a conservative approach, removing data points that are four standard-deviations above or below the mean of a running window of 30 days. Finally, data measured under poorly developed turbulent conditions (u*-filtering) was filtered out with the R-package REddyProc V. 1.3.2 (Wutzler et al., 2018) using RStudio version 2025.09.02. To estimate the range of possible u*-thresholds, the probability distribution of the threshold was estimated from 100 bootstraps, and estimates spanning from the 0.05 to the 0.95 quantiles were extracted. All further processing steps (gap filling and partitioning) were repeated for all these potential u*-thresholds to allow an estimation of the uncertainty associated with the choice of this threshold.

In order to derive annual budgets of fluxes the gaps resulting from the above-described steps needed to be filled. Deep ensembles of neural networks to fill gaps in CO_2 and CH_4 fluxes yield good predictive performance as well as reliable estimates of the respective model uncertainties (Vekuri et al., 2025). We trained an ensemble of five neural networks (Lakshminarayanan et al., 2017) for each u*-threshold to predict half-hourly CO_2 and CH_4 fluxes. The predictors used were TA, VPD, SWIN and fuzzy variables derived from the hour and the month turned into sine and cosine waves. During model training 20% of data was set aside as test data to evaluate the model performances. We followed a model setup previously shown to yield good flux predictions (Vekuri et al., 2025) using the Tensorflow library (Martín Abadi et al., 2015). The models consist of two hidden layers with 50 nodes each and ReLU (Rectified Linear Unit) activations. Since flux errors were shown to approximately follow a Laplace distribution (Hollinger & Richardson, 2005) the loss function of the model was the Laplace negative log likelihood. The models are trained to predict the mean and the logarithm of the scale parameter of a Laplace distribution, yielding a mean prediction as well as the predictive uncertainty. Following (Vekuri et al., 2025) the models were initialized with random weights (K. He et al., 2015) using the Adam optimizer (Kingma & Ba, 2014). A randomly sampled subset corresponding to 10% of the data was used as a validation set for early stopping with a patience of 20 epochs. The final gap filling uncertainty consists of the epistemic uncertainty, the uncertainty across the predicted means from the five model iterations, and the aleatoric uncertainty, the mean of the predicted Laplace scale parameters, added in quadrature.

Uncertainty for the final half hourly fluxes was computed by adding the uncertainties arising from the random measurement errors (Finkelstein & Sims, 2001), the uncertainty arising from the choice of u*-threshold (Pastorello et al., 2020) and the inherent gap filling model uncertainties (Vekuri et al., 2025).

https://doi.org/10.5194/egusphere-2026-1496
Preprint. Discussion started: 20 March 2026

Finally half-hourly filled CO_2 was partitioned into the two components of gross primary production (GPP) and ecosystem respiration (Reco) using the night-time partitioning approach (Reichstein et al., 2005). Daily NEE, GPP and Reco were derived from the half-hourly data as daily averages. As a quality control we tested the energy balance closure (EBC) of the flux data. The energy balance is calculated according to Eq. (1).

$$LE + H = (LWIN - LWOUT) + (SWIN - SWOUT) - SHF \quad (1)$$

It describes whether the measured fluxes of sensible (H) and latent (LE) heat flux together sum up to the total energy input into the ecosystem measured by the instrumentation minus the soil heat flux (SHF). The linear slope between the left and right side of Eq. (1) resembles the EBC and is used as a quality criterion of the fluxes (Foken, 2008). Typical values are around 0.8 (Mauder et al., 2024). The footprint of the tower was estimated using a two-dimensional flux footprint model (Kljun et al., 2015).

2.4 Detection of seasonality

The seasonality and dates of key phenological changes (start of season, SOS; peak of season, POS; end of season, EOS; length of season, LOS) were calculated based on the annual course of the GPP partitioned from NEE. We derived the change dates from a fitted double logistic sigmoid function (X. Zhang et al., 2003):

$$GPP(t) = \frac{L1}{1 + \exp\left(-k1 \cdot (t - t0)\right)} + \frac{L2}{1 + \exp\left(-k2 \cdot (t - t1)\right)} \quad (2)$$

where t represents the numeric index of the time series, L1 and L2 are the times of the early summer and later summer plateauing of GPP, k1 and k2 are the parameters for the curvature of the transition parameters and t0 and t1 control the midpoints of the transition periods. The change dates were determined by calculating the third derivative of Eq. (2). The date of the first local maximum and the last local minimum were taken as the start and end dates of the season. The peak of the season was determined as the date of the maximum of the fitted function. The seasons were then defined such that the non-growing season (NGS) is before and after the start and end of the growing season, early growing season (EGS) is between the start and the peak, and late growing season (LGS) between the peak and the end of the growing season.

2.5 Calculation of anomalies

To compare the climate and fluxes between the three years, anomalies of daily fluxes and climate were calculated using a block-averaging method. Each anomaly was calculated as the deviation of a data point from the mean of all available observations within a ±3 day-of-year window across all three years. Such anomalies were calculated for NEE, GPP, Reco, TA, SWIN, and VPD and are in the following denoted as z with the respective variable as subscript, e.g. z_{NEE}.

https://doi.org/10.5194/egusphere-2026-1496
Preprint. Discussion started: 20 March 2026

2.6 Driver Analysis

The drivers of gas fluxes at a daily timescale were analysed using forward stepwise multiple linear regression models (MLR) between the anomalies of daily fluxes and anomalies of environmental drivers. As the potential drivers of the fluxes z_{SWIN}, z_{TA}, z_{VPD} and z_{WTD} were included. Additionally, we added multiplicative interaction terms between all drivers as predictor candidates. Interaction terms are in the following denoted with a colon between two variables (e.g. z_{TA}:z_{SWIN}). In order to compare the relative influence of the drivers all predictors were standardized to the range of zero to one before fitting the model. Separate models were trained for the targets z_{NEE}, z_{Reco} and z_{GPP}. Predictors were sequentially added to the model. First the predictor was checked for collinearity. If the variance inflation factor (VIF) was larger than five the predictor was rejected. Second, if the model did not improve in its Akaike Information Criterion (AIC) and the adjusted R^2 did not improve at least by 0.05 the predictor was also rejected. Since driver strengths are likely to change between the non-growing and through the growing season, e.g. due to phenological development, separate models were created for the different seasons (see section 2.4). All models were built in Python version 3.7. MLR models were built using statsmodels version 0.14.6 (Seabold & Perktold, 2010). Preprocessing of the data made use of the scikit-learn package version 1.8 (Pedregosa et al., 2011).

2.7 Detecting physiological changes in Reco and GPP responses

Monthly changes in amounts of carbon fluxes may simply be caused by climatic differences while the underlying response functions remain the same. To test whether the environmental response of GPP or Reco fundamentally changed across the years, we established monthly temperature- and light-response functions.

We derived the temperature dependency of respiration as the Q10 value by fitting an exponential Lloyd-Taylor model (Lloyd & Taylor, 1994) to night-time CO_2 fluxes (NEE_{night}) with Eq. (3). NEE_{night} is used instead of the partitioned Reco because daytime Reco is already modelled based on a TA response curve.

$$NEE_{night}(T) = Rref \cdot exp\left(E0 \cdot \frac{1}{Tref - T0} - \frac{1}{T - T0}\right) \quad (3)$$

f is the baseline respiration rate at reference temperature, *T0* the baseline temperature set to -46°C, *Tref* the reference temperature (set to 10°C) and *E0* the activation energy parameter that determines the temperature dependency of the model. After the determination of *E0*, the temperature response parameter Q10, depicting the change of respiration with a 10°C change in temperature, is calculated with Eq. (4).

$$Q10(T) = exp\left(E0 \cdot \frac{1}{T-T0} - \frac{1}{T+10-T0}\right) \quad (4)$$

determine the light response of the ecosystem fluxes we fit a Michaelis-Menten rectangular hyperbolic light-response model (Bao et al., 2019; Falge et al., 2001) to daytime net ecosystem productivity (NEP) using Eq. (5). NEP is the inverse of NEE, which places net CO_2 uptake as positive values, making the positive relationship with increasing radiation more intuitive to interpret. Daytime data were defined as periods with incoming solar radiation of more than 50 W/m².

https://doi.org/10.5194/egusphere-2026-1496
Preprint. Discussion started: 20 March 2026

$$NEP(SWIN) = \frac{\alpha \cdot SWIN \cdot P_{max}}{\alpha \cdot SWIN + P_{max}} - Rd \quad (5)$$

α is the light-use efficiency (µMol J^{-1}), the initial slope of the curve representing the efficiency of carbon taken up per quantum of light respectively. P_{max} is the maximum rate of CO_2 uptake (µMol m^{-2} s^{-1}) and Rd (µMol m^{-2} s^{-1}) represents daytime ecosystem respiration.

2.8 Detecting the response of ecosystem carbon fluxes during high TA and VPD conditions

Detecting the effects of TA and VPD on carbon fluxes is complicated by their mutual correlation and co-variation with other drivers such as SWIN. We therefore employed a sequential filtering approach to isolate the effect of each variable while controlling for the others (Fig. S1). Half-hourly fluxes were first filtered for daytime conditions (SWIN > 50 W/m^2) and then for near light-saturated GPP using the 80th percentile of SWIN (570 W/m^2). Optimum conditions (VPD_{opt} and TA_{opt}) were determined using boundary line regression, in which GPP is grouped into 1°C bins, 1 hPa bins respectively, and separate regression lines are fit to percentiles from those bins (0.55–0.95, steps of 0.1), capturing the maximum GPP response envelope. VPD_{opt} and TA_{opt} were defined as the bin where the highest three consecutive percentile regressions reached their maximum (tolerance: ±1 bin). Data were then filtered to retain only conditions above these optima, as these are the ranges where a potential impact of TA or VPD can be expected.

To evaluate the effect of high TA while controlling for VPD (and vice versa), data were filtered to a narrow window of the controlled variable, with the window size selected as the largest window showing no detectable correlation ($p > 0.05$) of the controlled variable with the flux (tested from 0.5 to 6.5°C or hPa; Fig. S2). For the TA analysis, the VPD window was centred on the mean VPD of data with TA above the 50th percentile of TA > TA_{opt} (window: ±2.1°C). For the VPD evaluation, TA was centred on the mean TA of data with VPD above the 90th percentile of VPD > VPD_{opt} (window: ±5 hPa; Fig. S2). The different percentiles were required to capture high conditions of the evaluated variable and enable the removal of the correlation with the controlled variable while capturing enough data for a regression analysis. Finally, OLS regressions (statsmodels v0.14.6; Seabold & Perktold, 2010) were used to quantify the effect of TA or VPD on Reco, GPP and NEP, with separate models for the early and late growing seasons (see Section 2.4).

3. Results

3.1 Climate data and interannual variability

The additional meteorological data used to supplement the data measured at the EC tower completed the data with a high level of agreement. The R^2 of the linear models between secondary sources and the data measured at the EC tower was more than 0.9 for TA and RH from the auxiliary tower. For TA from the nearby DWD station it was 0.96 and for RH 0.8. The R^2 of the linear model between ERA5land derived surface solar downward radiation and the station SWIN was 0.88.

https://doi.org/10.5194/egusphere-2026-1496
Preprint. Discussion started: 20 March 2026

Over the three years the mean annual TA stayed between 11.6°C and 11°C (Fig. 2a). Annual mean radiation was also in a close range between a maximum of 124 kW/m² in 2025 and a minimum in 2024 with 116 W/m² (Fig. 2c). Both in 2023 and 2024 the site experienced exceptionally high amounts of precipitation with 1006 and 913 mm total rainfall (Fig. 2b), compared to a long-term average of 791 mm (2006–2025 reference period, data from the German meteorological station Ahaus, station ID 7374). Mean annual WTD tracked annual precipitation, averaging 25 cm depth in the two wet years (2023 and 2024) and reaching its deepest level at 37 cm in the driest year, 2025 (Fig. 2d).

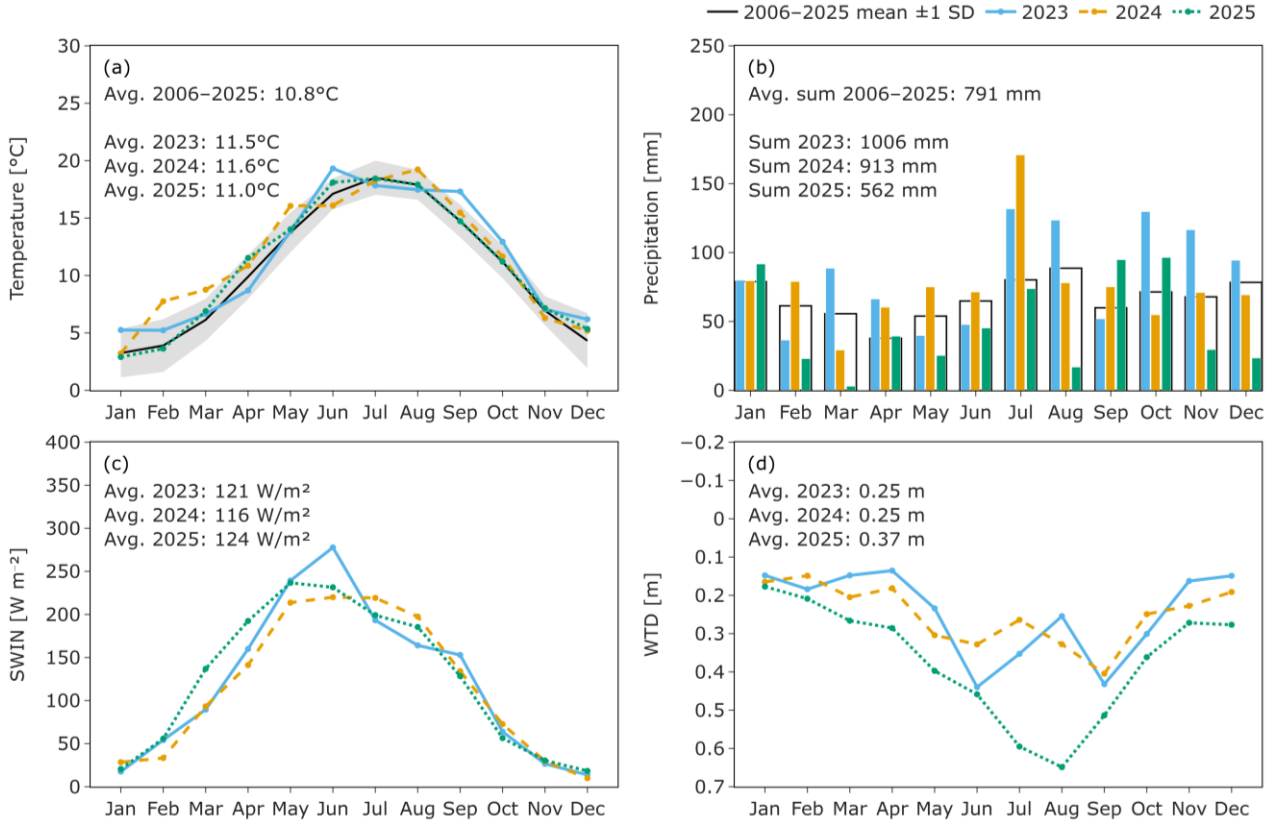

Figure 2: Monthly mean values of air temperature (TA), water table depth (WTD) and global radiation (SWIN) and sums of monthly precipitation (P) across the three measurement years. The grey band in (a) and the black background bar in (b) show the mean monthly and annual P and TA from 2006 until 2025 at a nearby station operated by the German meteorological service. Annotations show the annual means of TA (a), SWIN (c) and WTD (d), the annual sums of P (b) and the long-term averages of TA (a) and P (b).

Comparing the individual months between the years revealed more striking meteorological differences. In 2024 the average TA in February, March and May was 7.7°C, 8.8°C and 16.1°C, making each of these months the warmest among the three years by a margin of at least 2°C (Fig. 2a). In 2023 on the other hand the end of the growing season was the warmest among

https://doi.org/10.5194/egusphere-2026-1496
Preprint. Discussion started: 20 March 2026

the three years by more than 1.5°C at a mean of 17.3°C and 12.9°C in September and October. June 2023 was the warmest month of the three years with a mean monthly TA of 19.3°C, 3.1°C above the long-term average of 16.2°C (Fig. 2a).

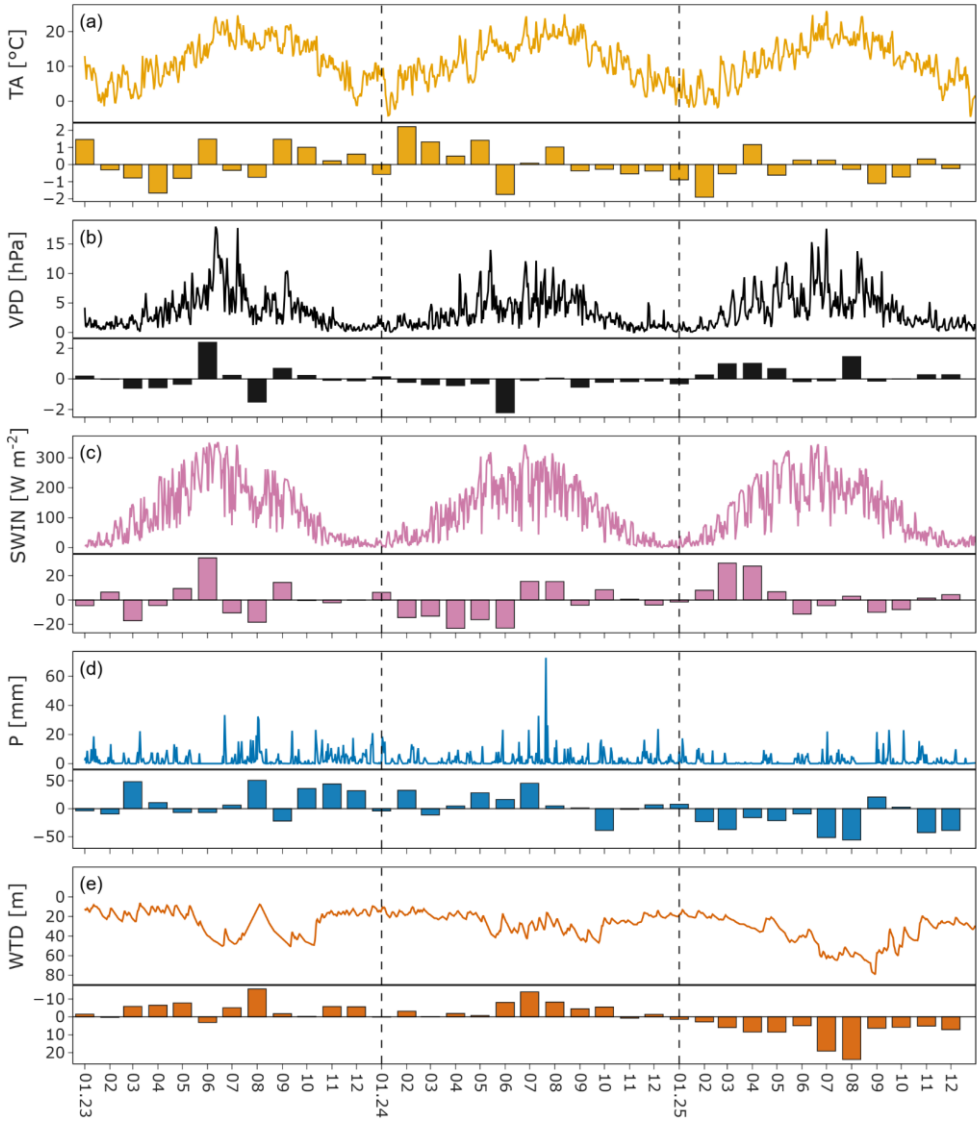

Figure 3: Daily time series and monthly anomalies of climate and hydrology in the three years. Bar plots below each time series show the monthly anomalies as the deviation of that month's mean from the mean across all three years. The y-axis of the WTD plot is reversed to resemble the WTD falling below the surface with increasing WTD. WTD data was partly derived from data provided by the Thünen Institute for Smart Agriculture as part of the Moorbodenmonitoring (MoMoK) project.

While annual cumulative rainfall was above average in both 2023 and 2024 (139% and 126% of the 20-year average; Fig. 2b), monthly distribution differed notably. In 2023, May and June were drier than usual (74% and 51% of average, while in 2024 March was the driest month (47%) and July the wettest (171 mm; 220% of average; Fig. 2b). The annual average WTD

https://doi.org/10.5194/egusphere-2026-1496
Preprint. Discussion started: 20 March 2026

in 2024 was similar to that in 2023. The lack of precipitation in May and June 2023 correlates with a sudden drop from 13.4 cm depth in April to 44 cm in June (Fig. 3d-e). In 2025 the year started with a precipitation deficit in March with only 3 mm, representing a 95% reduction compared to the long-term average (Fig. 2b). 2025 was by far the driest among the three years, with March, May, June, and August all experiencing less than 50% of the long-term average rainfall. Accordingly, the water table dropped earlier in 2025 and reached the highest depths of more than 60 cm (Fig. 3e), resulting in a lower mean annual WTD of 37 cm.

3.2 Quality of EC measurements

The EBC expressed as the slope between the sum of energy fluxes and the radiation budget minus the soil heat flux was 0.85 (Fig. S3) for the 2023–2025 study period, which is slightly higher than the average closure found for the FLUXNET2015 dataset (Mauder et al., 2024). Due to filtering steps and gaps in the original data in total 35% of CO_2 flux datapoints were filtered out, 53% of the night-time and 15% of the day-time fluxes respectively. Two events discontinued gas flux measurements in mid-summer, a lightning strike near the station in 9th of July 2023 that broke the datalogger, as well as substantial damage caused by rodents on 30th of June 2024 that led to a short-circuit, damaging controllers, gas analysers and soil sensors. The two incidents led to gaps of 19 and 29 days in 2023 and 2024, respectively. The ensemble neural networks filled the gaps with an average R^2 across all u*-scenarios of 0.85±0.03, uncertainty in the R^2 expressed as the 95% confidence interval across all models.

For CH_4 fluxes 70% of datapoints were filtered out. Fluxes remained very low during the study period with the 25th to 75th quantile ranging from -8.6 to 4.78 mmol m^{-2} s^{-1}. The fluxes barely exceeded the uncertainty of the measurements, with the random measurement uncertainty alone ranging from 2.3 to 6.3 mmol m^{-2} s^{-1}. Because the CH_4 fluxes were so low and irregular no correlations with environmental or meteorological variables were found. The tested gap filling algorithms yielded an R^2 on test data of near zero making the annual CH_4 budget highly uncertain. A driver analysis was therefore impossible.

3.3 Identification of vegetation growing season

The identification of the growing season revealed notable differences in timing of the start and end among the three years (Fig. 4). In 2024 the growing season started earliest, already on 20th of March or day-of-year (DOY) 80 (Fig. 4b). In 2023 in comparison the growing season onset was detected 23 days later, on 13th of April (Fig. 4a). The start of the growing season 2025 fell in between the other two years, eight days after the onset in 2024 on DOY 88 (Fig. 4c). For each year the other seasonal transitions shifted along with the onset of the growing season. 2023 had the latest start of the growing season but also the latest peak at day 198 (17th of July), 4 days later than in 2025, and the latest end of the growing season at DOY 320 (16th of November), one week after the second latest in 2025 (Fig. 4a). In 2024 the growing season started earliest, and it

https://doi.org/10.5194/egusphere-2026-1496
Preprint. Discussion started: 20 March 2026

also ended earliest on DOY 302 on 27th of October (Fig. 4b). In total the growing season lengths were therefore similar with 217, 222 and 225 and 2023, 2024 and 2025 respectively.

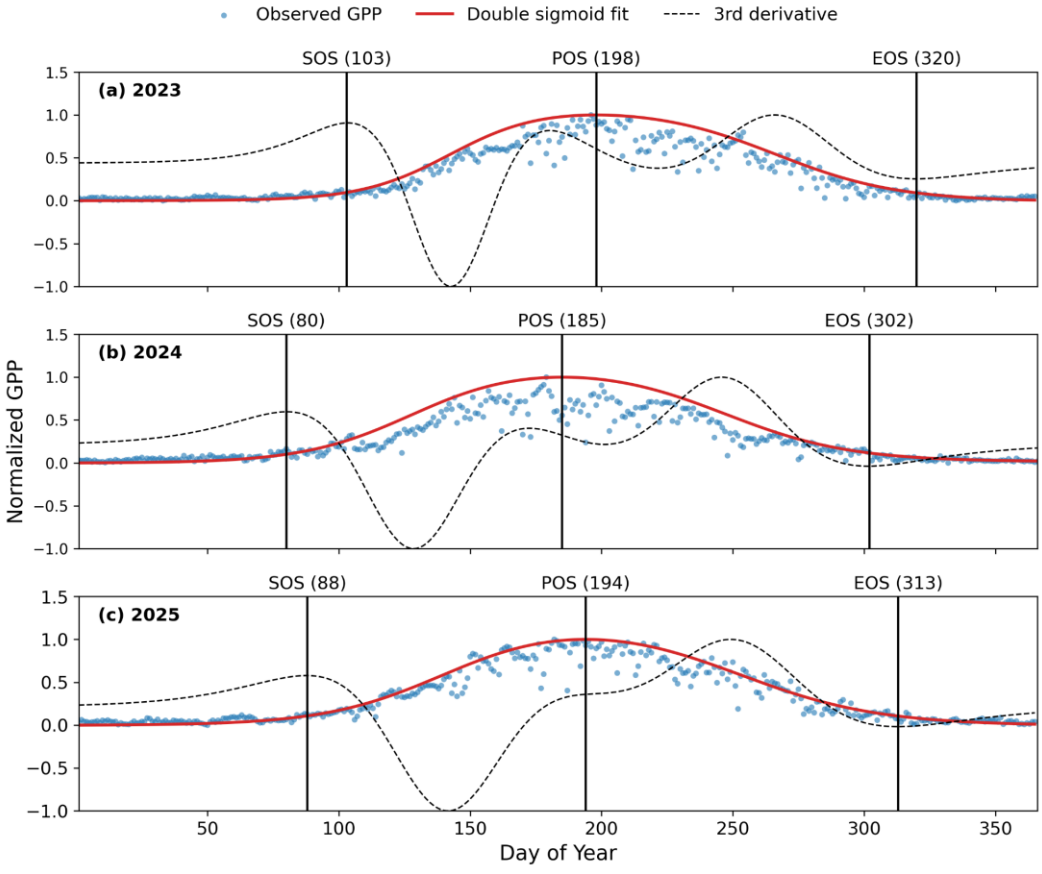

Figure 4: The growing and non-growing seasons in the three studied years. Blue dots show normalized daily mean GPP. The red line depicts the double-sigmoid curve fit and the dashed black line the respective third derivative. Vertical bars show the seasonal transitions with the day of the year in brackets notated on top. SOS is the start of season at the first maximum of the third derivative, POS the peak of season at the maximum of the double-sigmoid fit, and EOS the end of the growing season at the last minimum of the third derivative.

3.4 Annual, seasonal and monthly cumulative carbon fluxes

In the three measurement years the CO_2 budgets switched from a net source in 2023 with 131.9±17.2 gC m^{-2} to near CO_2 neutrality in 2024 with -5.7±19.9 gC m^{-2} (Table 1). In 2025 the site was a net CO_2 source again with emissions of 83.5±22.2 gC m^{-2} (Table 1). In 2024, where the ecosystem was in effect carbon-neutral, Reco was ca. 120 gC m^{-2} higher than in the previous year 2023. GPP however increased by 264 gC m^{-2} from 1337.5±45.2 gC m^{-2} to 1601.1±18.2 gC m^{-2}, surpassing Reco. In 2025 both Reco and GPP were lower than in the previous years with 1298.8±14.6 and 1215.3±11.1 gC m^{-2}.

https://doi.org/10.5194/egusphere-2026-1496
Preprint. Discussion started: 20 March 2026

The NGS was a CO2 source in all years, with relatively low interannual variability (maximum difference of 33 gC m^{-2} between 2023 and 2025; Table 1). The growing season (GS) was a net CO2 sink in all years, with substantially higher interannual variability: NEE ranged from −132.9±14.3 gC m^{-2} in 2024 to near-neutral in 2023 (−2.3±13.5 gC m-2), a difference of 131 gC m^{-2}. Reco and GPP were both higher in the GS than the NGS across all years. GS Reco ranged from 1134±9.9 gC m^{-2} to 1378±21.3 gC m^{-2}, GPP ranged from 1152±8.7 gC m^{-2} to 1511.7±17.4 gC m^{-2}, with both peaking in 2024. Interannual variability in GS carbon fluxes was higher than in the NGS, with Reco differing by up to 244 gC m^{-2} and GPP by up to 360 gC m^{-2} between years. NGS Reco was less variable, ranging from 164 to 217 gC m^{-2}.

Table 1: Annual and seasonal budgets of net ecosystem exchange of CO_2 (NEE) and CH_4, ecosystem respiration (Reco) and gross primary production (GPP). Seasons are defined as the non-growing season (NGS), early growing season (EGS) and late growing season (LGS) as described in Sect. 2.4.

Year	Season	NEE [gC m^{-2}]	Reco [gC m^{-2}]	GPP [gC m^{-2}]	CH_4 [gCO_2-C eq. m^{-2}]
2023	Annual	131.9±17.2	1468.7±49.9	1337.5±45.2	-
	NGS	133.8±4.9	201.9±6.2	68.0±5.3	-
	GS	-2.3±13.5	1267.1±43	1269.4±38.8	-
2024	Annual	-5.7±19.9	1595.4±22.7	1601.1±18.2	-8.5±114.9*
	NGS	127.1±4.3	216.9±1.7	89.7±1.2	-
	GS	-132.9±14.3	1378±21.3	1511.7±17.4	-
2025	Annual	83.5±22.2	1298.8±14.6	1215.3±11.1	-6±1750*
	NGS	100.4±4.9	164.2±4.7	63.8±3.7	-
	GS	-16.8±15.8	1134±9.9	1151.5±8.7	-

* CH_4 fluxes were very low and showed almost random behaviour, leading to small and highly uncertain budgets, thus a seasonal differentiation was not feasible.

In 2024 CO_2 uptake started earlier and was stronger compared to the other two years (Fig. 5a-b). Thus, during the peak of the growing season in August, in 2024 an intermediate maximum net uptake of as much as 130 gC m^{-2} was reached, while in 2023 the cumulative CO_2 flux barely reached a net uptake at any time (Fig. 5a). In 2025 GPP started slightly earlier and was stronger in May and June compared to 2023, but both Reco and GPP also declined faster starting August and September. Overall lower fluxes in 2025 led to significant emissions which were however lower than in 2023.

https://doi.org/10.5194/egusphere-2026-1496
Preprint. Discussion started: 20 March 2026

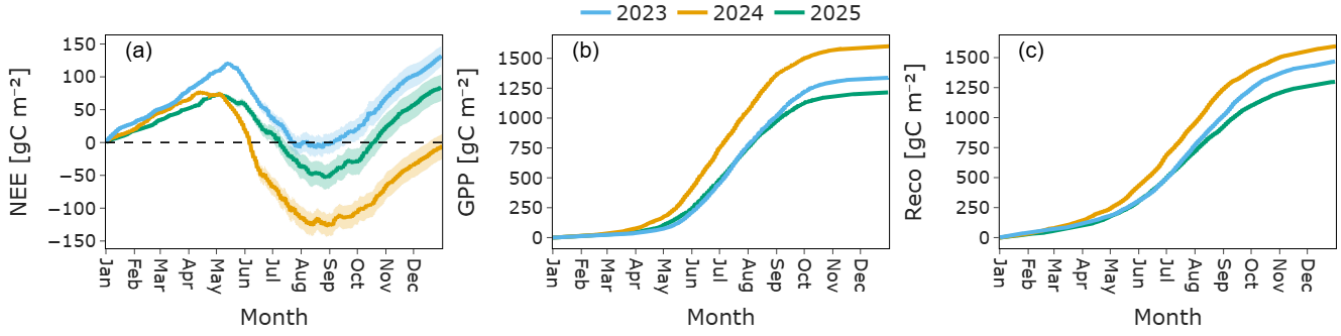

Figure 5. Cumulative sums of net ecosystem exchange (NEE, A), gross primary production (GPP, b) and ecosystem respiration (Reco, c). Uncertainty bands denote the 95% CI of the cumulative values.

The monthly flux budgets reveal the decisive periods for the differences in the annual carbon budgets (Fig. 6). The largest differences between the years occurred from April to June, after which monthly NEE was similar across years (Fig. 6a). Most striking is April to June 2024, where both Reco and GPP were strongly increased (Fig. 6b-c) compared to the other years, with GPP rising more than Reco. This led to reduced net emissions in April 2024 and a marked increase in net CO_2 uptake in May and June 2024 (Fig. 6a).

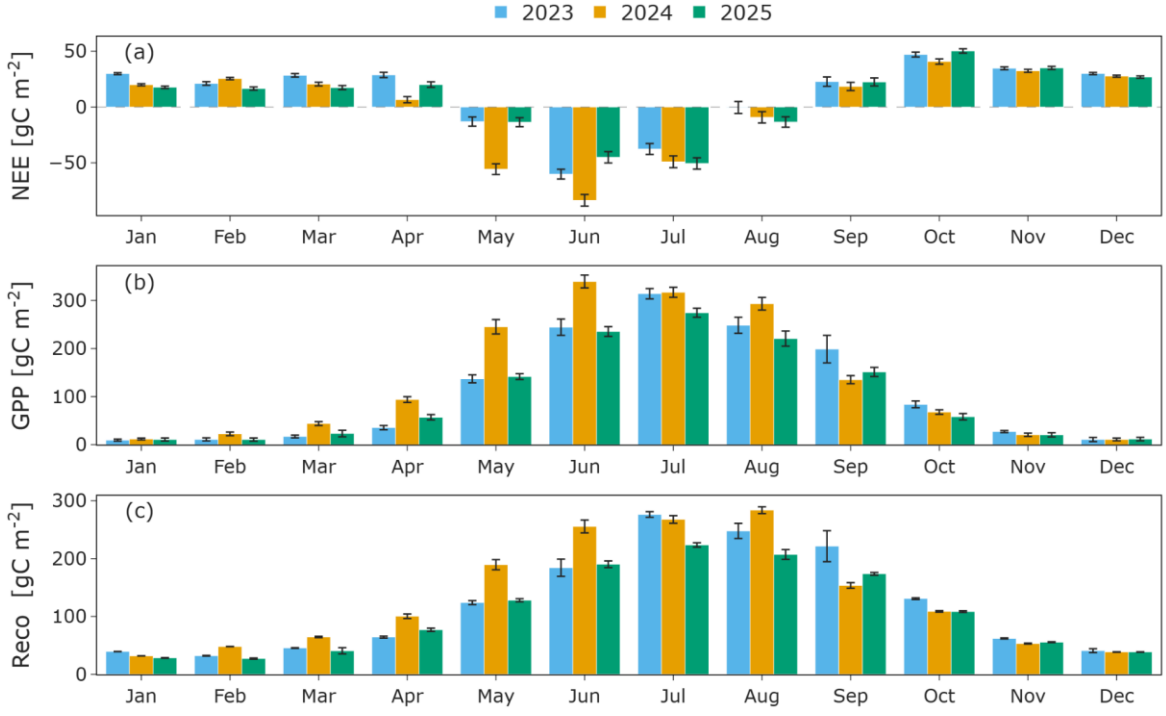

Figure 6. Monthly sums of fluxes of NEE (a), GPP (b) and Reco (c). Error bars denote the 95% CI of the monthly sum.

https://doi.org/10.5194/egusphere-2026-1496
Preprint. Discussion started: 20 March 2026

The high total emissions of 2023 were accompanied by higher net emissions in March and April and lower net uptake in July and August than in the other years (Fig. 6a). From February to August, GPP and Reco were both largest in 2024, apart from July, where Reco was higher in 2023.

3.5 Driver analysis of daily flux anomalies per season

The multiple linear regression model performance varied considerably among seasons and target flux anomalies. In the non-growing season, the models for z_{Reco} and z_{NEE} explained a large share of the variance (R^2 = 0.67 and 0.82), while z_{GPP} was poorly captured (R^2 = 0.32), however this is expected as GPP is mostly absent in the NGS. The early growing season showed the lowest model performance across all seasons, with R^2 ranging from 0.25 for z_{GPP} to 0.41 for z_{NEE}, thus daily climate anomalies alone explain a smaller share of flux variability during this period. In the LGS z_{NEE} and z_{GPP} were well explained (R^2 = 0.76 and 0.63) and models for z_{Reco} showed moderate performance (R^2 = 0.59).

The selected predictor variables varied for each flux between the seasons (Fig. 7). For z_{NEE} the strongest driver of increasing emissions was z_{TA} in the NGS and LGS, thus higher TA increased net CO_2 emissions (Fig. 7a). Notably the effect of z_{TA} was reduced in the EGS. During the EGS, the interaction of anomalies in VPD and SWIN instead emerged as the strongest driver of increased NEE (thus increased emissions or decreased CO_2 uptake). In contrast, anomalies in incoming radiation (z_{SWIN}) were the strongest driver of increased CO_2 uptake across all seasons. Concurrent conditions of warm TA and high light availability (thus the interaction z_{TA}:z_{SWIN}) exerted an additional uptake-enhancing effect throughout the year.

z_{Reco} was primarily controlled by z_{TA} across all seasons, with warmer conditions consistently driving enhanced Reco (Fig. 7b). A secondary positive effect of z_{WTD} indicated that drier conditions also increased Reco, particularly during the growing season. Conversely, positive VPD anomalies suppressed Reco, most strongly during the EGS. Remaining significant effects were very small across all seasons (coefficients < 0.1).

Increased GPP was associated with positive anomalies in SWIN, TA, and WTD, alongside the interaction of z_{TA}:z_{SWIN} (Fig. 7c). Increased incoming solar radiation (z_{SWIN}) had the strongest positive effect on GPP in the LGS and a markedly weaker effect in the EGS. The influence of z_{TA} was largest in the non-growing season, likely reflecting uptake extending beyond the formally derived growing season boundaries. The influence of the interaction z_{TA}:z_{SWIN} also varied through the year, with its lowest effect in the LGS. Across all seasons, the interaction z_{VPD}:z_{SWIN} exerted a negative effect on GPP, with a stronger impact in the EGS than the LGS, suggesting a negative impact of VPD on CO_2 uptake under light-saturated conditions

https://doi.org/10.5194/egusphere-2026-1496
Preprint. Discussion started: 20 March 2026

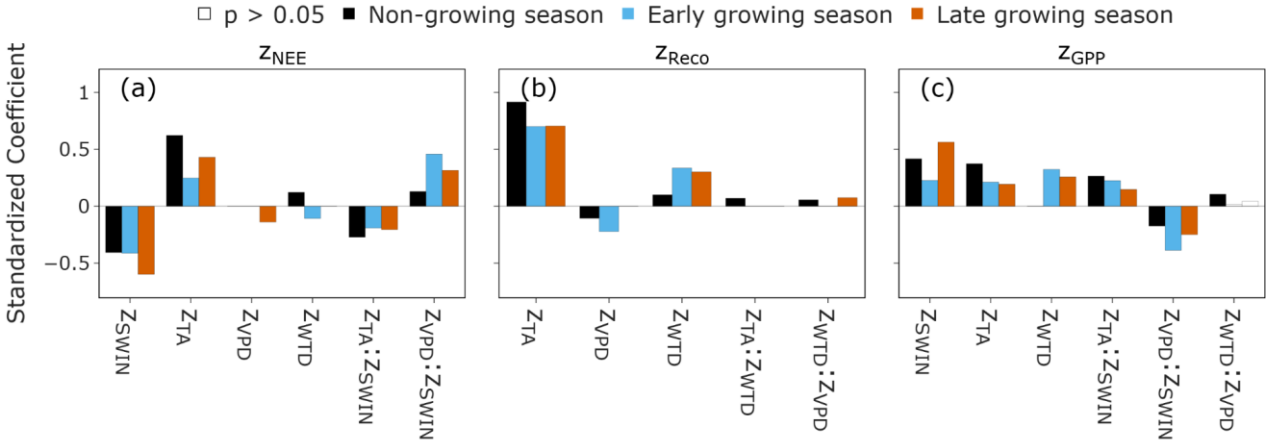

Fig. 7: Coefficients of stepwise-forward MLR models with anomalies of NEE (a), Reco (b) and GPP (c) as target variables and anomalies in climate and environmental ancillary variables as well as their interactions as predictors. Models are fit for the non, early and late growing season separately. Coefficients selected during the stepwise-forward procedure but that are non-significant are shown in white with black orders (z_{VPD} in the LGS in B).

3.6 Photosynthetic and Respiratory Controls on CO_2 Exchange

Light-use efficiency α and P_{max} show a typical seasonal cycle with P_{max} reaching up to 37 µMol m^{-2} s^{-1} in June and July (Fig. 8). In April, May and June 2024 P_{max} was strongly increased with 13, 26 and 38 µMol m^{-2} s^{-1} (Fig. 8b) compared to an average of 5, 14 and 25 µMol m^{-2} s^{-1} in the other two years. Further, the light-use efficiency in May 2024 was higher than in the other years with 0.21 µMol J^{-1} compared to 0.04 µMol J^{-1} and 0.1 µMol J^{-1} in 2023 and 2025 respectively. From June to August 2024, the Q10 of respiration was higher compared to the other years with a mean of 1.8 across the three months compared to 1.4 in the other two years and a maximum of 2.1 reached in June 2024. In August 2025 both P_{max} and the Q10 of respiration are notably lower than in the other two years with a Q10 of 1 compared to 1.4 and 1.6 and a P_{max} of 26 µMol m^{-2} s^{-1} compared to 34 µMol m^{-2} s^{-1} in the other two years.

https://doi.org/10.5194/egusphere-2026-1496
Preprint. Discussion started: 20 March 2026

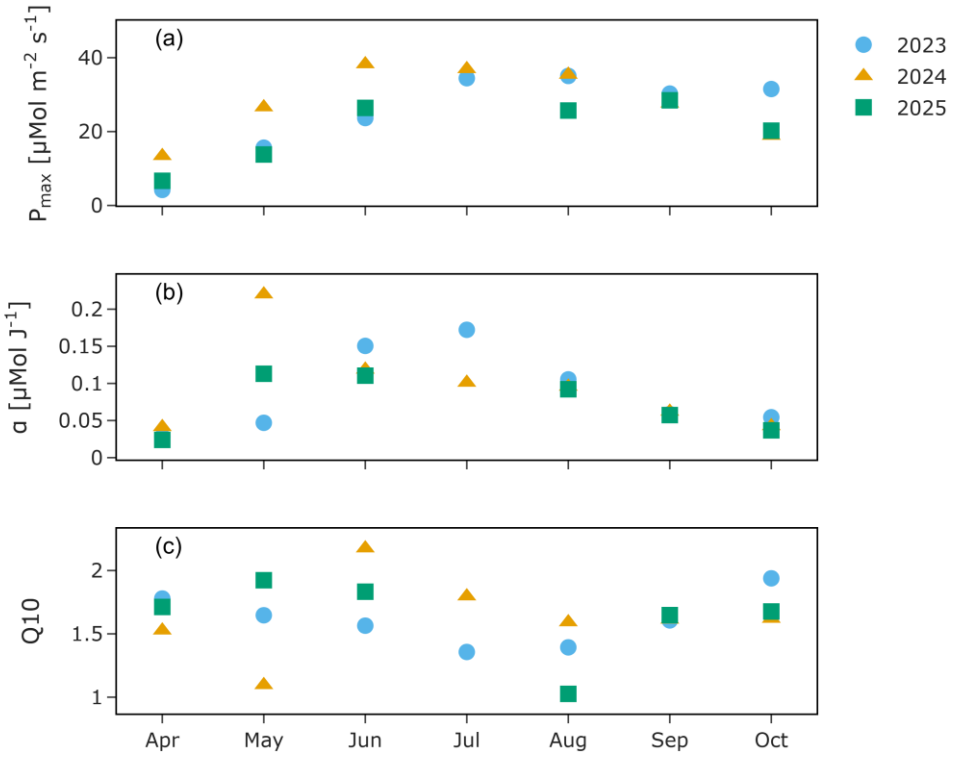

Figure 8: Maximum photosynthetic uptake capacity P_{max} (a) and light-use efficiency α (b) derived from light-response-curves for NEP as well as the temperature sensitivity of night-time NEE Q10 (c), derived from a Lloyd-Taylor model. Light-response and Lloyd-Taylor models are fit for each month in each year separately.

3.7 Ecosystem responses to elevated TA and VPD

The employed filtering methods successfully isolated the effects of TA and VPD, reducing all correlations controlled for to maximum remaining Pearson correlation coefficient of 0.13 (Fig. S4). Notably, a negative correlation ranging from -0.18 to -0.42 with SWC was found for all fluxes both in the data controlled for VPD and the data controlled for TA (Fig. S4), depicting increasing carbon fluxes under reducing soil moisture in the filtered data.

https://doi.org/10.5194/egusphere-2026-1496
Preprint. Discussion started: 20 March 2026

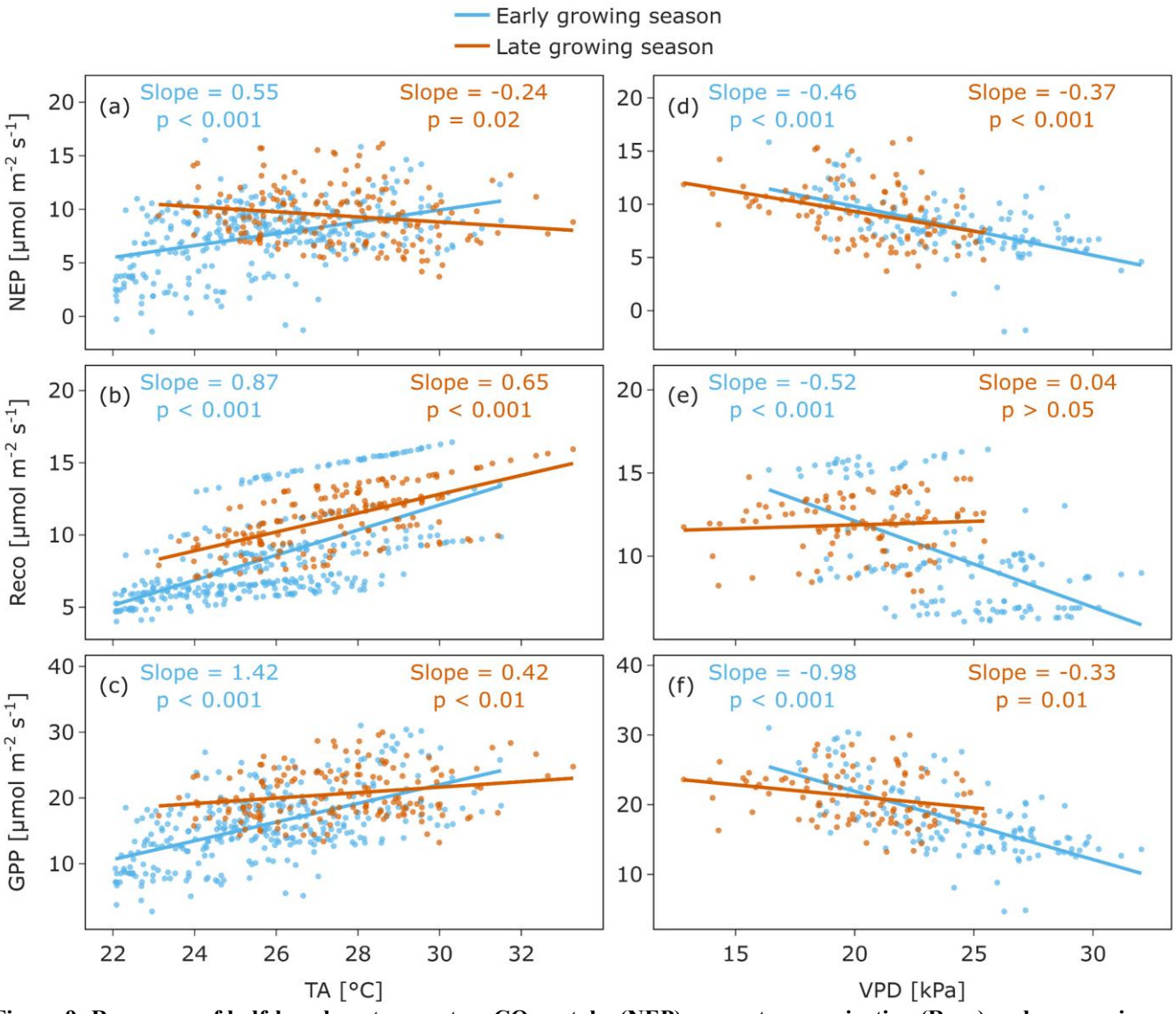

Figure 9: Responses of half-hourly net ecosystem CO_2 uptake (NEP), ecosystem respiration (Reco) and gross primary production (GPP) on high TA (A, B, C) and VPD (D, E, F) conditions. Data is filtered such that the respective effects of TA and VPD are isolated. Points and regression lines in blue depict the data from the early growing season (EGS), red is the data from the late growing season (LGS).

Throughout the growing season, even under highest encountered TA conditions warming was positively correlated with both GPP and Reco (Fig. 9a–c), but increased NEP in the EGS and decreased NEP in the LGS (Fig. 9a). In the EGS, GPP responded stronger to high TA than Reco (Fig. 9b, c), resulting in increasing net CO_2 uptake (Fig. 9a). In contrast, in the LGS Reco increased stronger with TA than GPP (slopes of 0.65 and 0.42, Fig. 9b, c), leading to a decreasing net CO_2 uptake (Fig. 9a).

https://doi.org/10.5194/egusphere-2026-1496
Preprint. Discussion started: 20 March 2026

Contrary to the TA response, VPD increasingly suppressed all fluxes in the EGS (Fig. 9d-f). The decrease of GPP under high VPD during the EGS was almost twice as strong as the reduction in Reco with a slope of -0.98 (Fig. 9f) compared to -0.52 (Fig. 9e). In the LGS the responses changed markedly. Reco was not significantly correlated with VPD while GPP was still reduced but the effect was weaker than in the EGS with a slope of -0.33 (Fig. 9f). Together the reduction of GPP and the absent reduction of Reco in the LGS also resulted in a decrease in NEP similar to the EGS (slope of -0.37 compared to -0.46, Fig. 9d).

4 Discussion

4.1 Annual and seasonal dynamics of carbon budgets

Annual CO_2 budgets were variable, ranging from a net source of 131 gC m^{-2} to near neutrality of -5 gC m^{-2} (Table 1). These values fall between IPCC CO_2 emission factors for rewetted temperate (-64 to 18 gC m^{-2}) and extraction peatlands (110 to 420 gC m^{-2}) (IPCC, 2014). According to the German CO_2 emission inventory for wetlands, our study site with a WTD of persistently more than 20 cm and shrub-dominated vegetation, falls in the category of drained unutilized land, where emissions are estimated within the range of 70 to 1080 gC m^{-2} (Tiemeyer et al., 2020). With mean annual emissions of 69 gC m^{-2} the measured annual budgets fall to the lower end of this estimation, confirming a moderate but real contribution to global warming.

Past studies found that either the variability in Reco (Aslan-Sungur et al., 2016; Drollinger et al., 2019; Ueyama et al., 2014) or in GPP (Chivers et al., 2009; Q. Li et al., 2021; Lund et al., 2010) controlled the annual variability of CO_2 budgets. In the three measurement years the variability of NEE in the growing season was substantially higher than in the NGS (131 gC m^{-2} and 33 gC m^{-2} maximum difference; Table 1) and the differences in GPP were greater than those in Reco (360 gC m^{-2} and 244 gC m^{-2} maximum difference respectively; Table 1). This highlights that the growing season vegetation activity played a pivotal role in shaping the interannual variability in CO_2 fluxes.

Ranges of annual GPP and Reco at Amtsvenn (1197–1595 and 1275–1588 gC m^{-2}, respectively) are high compared to other reported flux budgets from semi-natural bogs with shrubs in the footprint and similarly fluctuating water tables, where fluxes typically range between 600 and 800 gC m^{-2} (Humphreys et al., 2014; Hurkuck et al., 2016). The high GPP is likely attributable to the dense shrub canopy, as shrubs can sustain carbon uptake rates exceeding those of natural peatlands or even grasslands (Gyimah et al., 2020; Quin et al., 2015). Elevated Reco is consistent with the WTD persistently exceeding 15 cm, which promotes peat aeration and microbial decomposition (Ma et al., 2022; Swails et al., 2022). Additionally, Reco may be enhanced through vegetation activity. Root exudates released by ericaceous shrubs can increase CO_2 emissions by increasing the microbial potential for cellulose and hemicellulose decomposition (Cai et al., 2024) and autotrophic respiration, which can make up more than 50% of the total Reco in shrub dominated ecosystems (Rankin et al., 2023), increases with GPP (Waring et al., 1998).

https://doi.org/10.5194/egusphere-2026-1496
Preprint. Discussion started: 20 March 2026

Methane fluxes were low and did not exceed measurement uncertainty. CH_4 emissions require anoxic, waterlogged soils (Evans et al., 2021; Frolking et al., 2011; W. Zhang et al., 2022) and approach zero when annual average WTD is deeper than 20 cm (Calabrese et al., 2021; Evans et al., 2021), which was almost always the case in the three measured years (Fig. 3e). Repeated drying-rewetting cycles can further suppress CH_4 formation through regeneration of electron acceptors (Gao et al., 2019; Knorr et al., 2009). Although *Molinia caerulea*, which is present with up to 25% cover, could act as a methane conductor (Buzacott et al., 2024; van den Berg et al., 2020), shrub dominance and persistently deep water tables likely explain the absence of detectable CH_4 emissions.

4.2 Drivers of CO_2 fluxes

4.2.1 The impact of climate and hydrology on CO_2 fluxes

Net CO_2 uptake and GPP were strongly controlled by z_{SWIN}, which is expected as radiation is the primary driver of photosynthesis (Fig. 7a, c). Daily TA anomalies were a consistent driver of all CO_2 flux components. TA increased daily Reco more than GPP, resulting in a net emission-increasing effect (Fig. 7b, c). Past studies support decreased net uptake with rising TA through increased Reco especially in mid-summer (Aslan-Sungur et al., 2016; Drollinger et al., 2019; Poczta et al., 2023; Wilson et al., 2016), but sustained warming can also promote CO_2 uptake and growth of graminoids (Q. Li et al., 2021; Oestmann et al., 2022) and shrubs (Walker et al., 2015). The interaction z_{TA}:z_{SWIN} reduced NEE (Fig. 7a) and increased GPP (Fig. 7c), suggesting that under concurrently light-saturated and warm conditions net CO_2 uptake was indeed enhanced.

Anomalies in WTD had little influence on daily NEE and only during the non-growing season (Fig. 7), contrasting with its widely accepted role as the primary driver of CO_2 emissions across sites (Evans et al., 2021; Ma et al., 2022; Tiemeyer et al., 2020). On the daily scale both anomalies of GPP and Reco increased with anomalies in WTD, likely cancelling each other out in their effect on z_{NEE} (Fig. 7b, c). The positive relationship of WTD and GPP suggests that GPP was not limited by the prevailing WTD conditions. Previous studies found that at WTD of less than 50 cm shrubs are not limited by water availability (Farrick & Price, 2009; Lafleur, Hember, et al., 2005). This reported threshold of 50 cm fits to the observed reduction of P_{max} (Fig. 8a) and lower GPP (Fig. 6b) in July and August 2025 compared to the other years after a prolonged period of low rainfall with resulting mean monthly WTD deeper than 50 cm. Notably both Reco and Q10 of respiration were suppressed during the same period (Fig. 6c and Fig. 8c), pointing towards a strong coupling between vegetation activity and Reco, which could be provided through autotrophic respiration and the release of root exudates (Cai et al., 2024; de Vries & Caruso, 2016; Voigt et al., 2017). A concurrent direct moisture limitation of Reco may also cause the reduced Q10 (Estop-Aragonés & Blodau, 2012). Additionally, decades of drainage-induced peat decomposition — evidenced by C/N ratios of 30–40 and enrichment of refractory moieties (Lemmens et al., 2026) — may have reduced oxygen diffusivity in the upper peat layers (Hamamoto et al., 2016), further constraining the effect of WTD drawdown on decomposition at depth.

https://doi.org/10.5194/egusphere-2026-1496
Preprint. Discussion started: 20 March 2026

VPD and its interaction with SWIN emerged as important drivers of CO_2 fluxes. z_{VPD}:z_{SWIN} had a marked decreasing effect on GPP (Fig. 7c), likely caused by stomatal closure under high atmospheric dryness (Grossiord et al., 2020). This was also reflected in a net emission-promoting effect of z_{VPD} on anomalies in net CO_2 fluxes (Fig. 7a). Although TA and VPD are coupled, they may affect CO_2 fluxes independently. Under high TA, when moisture is not limiting, plants can cool their leaves by transpiring water, keeping their stomata open and continuing CO_2 uptake (Michaletz et al., 2016). High VPD on the other hand can suppress GPP even irrespective of soil moisture (Fu et al., 2022; Schönbeck et al., 2022). The contrasting effects of z_{TA}:z_{SWIN} (increasing uptake) and z_{VPD}:z_{SWIN} (decreasing uptake) (Fig. 7a, c) suggest a diverging response of the vegetation to high TA and VPD under light-saturation.

4.2.2 The effect of high VPD and TA conditions on sub-daily CO_2 fluxes

Both GPP and Reco increased with rising TA under extreme warm conditions (Fig. 9b-c). Temperature manipulation studies have shown that shrubs can benefit from warming and increase GPP (Munir et al., 2015; Ward et al., 2013), especially when the top peat layers become drier at the same time (Laine et al., 2019). A global synthesis of flux measurements and satellite-based indices found that on the ecosystem scale the optimum TA for GPP lies between 25°C and 30°C for temperate shrublands (Huang et al., 2019). Here we found no indication of a reduction of GPP up to conditions of 32°C (Fig. 9c). Whether rising TA under warmest conditions resulted in further increases or decreases in net CO_2 uptake depended on the different rates of increase in GPP or Reco rather than a limitation of either one (Fig. 9a). Our results provide no evidence that elevated TA up to 32°C alone limited GPP, e.g. through a stomatal closure in response to heat stress.

High VPD, in contrast to high TA, suppressed all carbon fluxes in the early growing season (Fig. 9d-f). Studies on the site-scale found that shrub-dominated canopies tend to leave stomata open during high VPD, exhibiting a "water-spending" behaviour (Gobin et al., 2015; Speranskaya et al., 2024). However, a meta study on global flux data found that shrublands are expected to react with decreased evapotranspiration and stomatal closure to increased VPD (Massmann et al., 2019). The reduction of GPP under rising VPD observed here points towards constrained gas exchange due to stomatal closure (Grossiord et al., 2020; Novick et al., 2024). The presence of individuals of *Betula* trees and up to 25% coverage of *Molinia caerulea*, which are known to react with stomatal closure to high VPD (Gobin et al., 2015; Osonubi & Davies, 1980; Otieno et al., 2012) likely contributed to the marked reaction of GPP to high VPD. Additionally, not only GPP but also Reco was suppressed under elevated VPD. A VPD-driven reduction in Reco is, to our knowledge, undocumented in the literature. Given that autotrophic respiration may constitute a substantial fraction (>50%) of Reco in shrub-dominated ecosystems (Rankin et al., 2023), growth suppression may explain the observed decreasing Reco. The effect of high VPD could be confounded if soil water stress occurs at the same time (Wang et al., 2022). However, in the data used for the inference of the VPD effect the correlation of SWC and carbon fluxes was negative (Fig. S4), meaning that fluxes increased with lower SWC. This makes a constraint through soil water depletion unlikely.

https://doi.org/10.5194/egusphere-2026-1496
Preprint. Discussion started: 20 March 2026

4.3 Timing of climate anomalies determines their impact on annual CO_2 budgets

Studies have produced varying results on whether climate warming increases or decreases net CO_2 uptake in northern peatlands, suggesting both increasing emissions of CO_2 and CH_4 into the atmosphere with warming (Hanson et al., 2020; Helbig et al., 2022; Qiu et al., 2022) or enhanced net CO_2 uptake, especially in boreal *Sphagnum*-dominated peatlands (Zhao et al., 2026). In this study annual budgets of both GPP and Reco were highest in the warmest year 2024 (Table 1, Figure 2A). A warm spring in 2024 (~2°C above other years from March to May) triggered an earlier growing season onset (DOY 80 vs. 103 in 2023, Fig. 4a-b) and a rapid GPP increase (Fig. 5b) despite lower radiation in 2024 (Fig. 3c), driving the site to near CO_2 neutrality. The higher GPP was accompanied by an increased P_{max} of up to 85% between April and June relative to the other years (Fig. 9). Enhanced CO_2 uptake following pre-growing season warming was previously found in both fens and bogs (Adkinson et al., 2011; Heiskanen et al., 2021; Helfter et al., 2015; Peichl et al., 2014). In contrast to a boreal fen where P_{max} increased with a lag in mid-summer following a warm spring (Peichl et al., 2014), P_{max} at Amtsvenn was already elevated at the onset of the growing season in April and May (Fig. 8a). This may reflect the capacity of the evergreen shrub canopy to respond immediately to warm conditions without the constraints of leaf development.

In contrast to the effect of the warm spring, during the warm autumn in September and October 2023 (Fig. 3a) the net CO_2 budget was not significantly different from the other years (Fig. 6a) because both Reco and GPP were similarly enhanced (Fig. 6b, c). The partitioned influence of TA further confirmed the different responses of CO_2 fluxes to high TA in the EGS and LGS. In spring warmer conditions enhanced net CO_2 uptake by stimulating GPP more than Reco, while autumn warming reduced net CO_2 uptake by increasing Reco more than GPP (Fig. 9a–c). The CO_2 flux response to high TA thus depended critically on seasonal timing, consistent with findings on the large scale across northern ecosystems (Barichivich et al., 2013; Helbig et al., 2022).

The impact of high VPD conditions also changed seasonally. Under rising VPD net CO_2 uptake was increasingly suppressed throughout the growing season (Fig. 9d). The effect of high VPD on net CO_2 uptake in the EGS and LGS was similar with slopes of -0.46 and -0.37. However, the individual responses of GPP and Reco differed drastically between the seasons. GPP was suppressed almost three times stronger (slope of -0.98 compared to -0.33) in the EGS than in the LGS (Fig. 9f). Reco on the other hand decreased with rising VPD in the EGS (slope of -0.52) and was not significantly correlated to VPD in the LGS (Fig. 9e). The decrease in Reco with rising VPD in the EGS thus reduced the impact of decreasing GPP on the overall net CO_2 balance and led to the similar response as in the LGS. To the best of our knowledge there is no study showing such a divergent response of CO_2 fluxes to high VPD conditions between early and late growing season periods controlled for concurrent changes in SWIN or TA. While seasonally varying TA impacts have received some attention (Bubier et al., 1998; Heiskanen et al., 2021; Helbig et al., 2022; Helfter et al., 2015) the seasonal trajectory of VPD impacts has not been systematically evaluated. A detailed analysis of the leaf- or plant-level mechanisms behind this divergence is beyond the scope of this study. It may however represent a process counteracting increased spring CO_2 uptake under future warming - particularly as extreme VPD and TA events are projected to intensify (Intergovernmental Panel on Climate Change (IPCC),

https://doi.org/10.5194/egusphere-2026-1496
Preprint. Discussion started: 20 March 2026

2023; Shekhar et al., 2024) and rising VPD is expected to place greater pressure on plant water regulation (C. Li et al., 2025; Novick et al., 2016).

Conclusions

CO_2 emissions from drained, vegetated peatlands can vary extremely across years, ranging from substantial net CO_2 sources to near neutrality under specific climatic conditions. Analysing CO_2 fluxes and their climatic drivers over three years revealed that seasonal timing of climate anomalies, rather than their magnitude alone, impacted the annual carbon balance. A prolonged warm spring in 2024 accelerated growing season onset and drove a rapid CO_2 uptake, temporarily compensating Reco and pushing the site toward carbon neutrality in that year. This sensitivity to spring warming, combined with the absence of detectable CH_4 emissions under persistently deep water tables, highlights how site-specific vegetation and hydrological conditions can modulate the response of annual carbon balances to warming in ways not captured by broad emission factor categories. Seasonal timing also governs the influence of other drivers: the negative effect of VPD on GPP in the early in the growing season was three times stronger than in the late growing season. That TA and VPD acted in opposition — warming advancing and amplifying carbon uptake while elevated VPD suppressed it — reveals how season-specific climate can produce different ecosystem responses. These findings warrant further research into how the seasonal timing of TA and VPD extremes shape carbon flux dynamics and how their seasonal occurrence will evolve under ongoing climate change.

While this study spans three years, the period captured substantial inter-annual variability, providing valuable insight into peatland responses to the climate. Continued observations over longer timescales would further strengthen the assessment of whether the observed patterns—particularly the spring warming response and the seasonal divergence in VPD effects—represent persistent characteristics of this ecosystem. We encourage combining complementary observations, such as biomass sampling, leaf-level conductance measurements, and root dynamics, with gas flux measurements in peatland ecosystems, to provide additional insight into the ecophysiological mechanisms underlying the observed gas fluxes. Such integrated approaches, applied across longer records and a broader range of peatland types and vegetation communities, would further enhance our understanding of the drivers of seasonal carbon dynamics.

Code Availability

Code will be made available upon request.

https://doi.org/10.5194/egusphere-2026-1496
Preprint. Discussion started: 20 March 2026

Data Availability

Amtsvenn is an ICOS associated site with the site code DE-Amv. The flux data and ancillary meteorological data are therefore accessible via the ICOS Data Portal at https://meta.icos-cp.eu/resources/stations/ES_DE-Amv

Author contributions

NB collected, processed, post-processed and curated all used data, conceptualized and conducted the analysis and wrote the original draft of the paper. MG acquired the funding, supervised the project and advised in developing the methodology and during the analysis. KHK provided resources in the form of meteorological, hydrological and peat chemical data. All authors reviewed and edited the manuscript.

Competing interests

The authors declare that they have no conflict of interest.

Disclaimer

Copernicus Publications remains neutral with regard to jurisdictional claims made in the text, published maps, institutional affiliations, or any other geographical representation in this paper. While Copernicus Publications makes every effort to include appropriate place names, the final responsibility lies with the authors. Views expressed in the text are those of the authors and do not necessarily reflect the views of the publisher.

Acknowledgements

We thank Simon Hofert and Andreas Malkus for their technical support in the field, Carsten Schaller for scientific and technical insights and Denise Rupprecht for conducting the vegetation survey. We extend our gratitude to the "Moorbodenmonitoring" project conducted by the Thünen Institute for Climate Smart Agriculture for providing us with their ground water table depth data, extending our own time series. AI tools (ChatGPT-4o, Sonnet 4.6) were used to assist with visualizations. All outputs were critically reviewed by the authors to ensure accuracy and integrity.

Financial support

NB was funded by the University of Münster Startup fund of the Junior Professorship for MG and EU-LIFE project CrossBorderBog. KHK acknowleges funding from 2020–2021 Biodiversa+ and Water JPI joint call for research projects, under the BiodivRestore ERA-NET Cofund (GA N ◦ 101003777), with the EU and the funding organisations DFG

https://doi.org/10.5194/egusphere-2026-1496
Preprint. Discussion started: 20 March 2026

(Germany), FWF (Austria), NCN (Poland; proposal nr. 2021/03/Y/ST10/00093) and the Ministry of LNV (The Netherlands).

References

Abadi, M., Agarwal, A., Barham, P., Brevdo, E., Chen, Z., Citro, C., Corrado, G. S., Davis, A., Dean, J., Devin, M., Ghemawat, S., Goodfellow, I., Harp, A., Irving, G., Isard, M., Jia, Y., Jozefowicz, R., Kaiser, L., Kudlur, M., Levenberg, J., Mané, D., Monga, R., Moore, S., Murray, D., Olah, C., Schuster, M., Shlens, J., Steiner, B., Sutskever, I., Talwar, K., Tucker, P., Vanhoucke, V., Vasudevan, V., Viégas, F., Vinyals, O., Warden, P., Wattenberg, M., Wicke, M., Yu, Y., and Zheng, X.: TensorFlow: Large-Scale Machine Learning on Heterogeneous Systems, 2015.

Adkinson, A. C., Syed, K. H., and Flanagan, L. B.: Contrasting responses of growing season ecosystem CO2 exchange to variation in temperature and water table depth in two peatlands in northern Alberta, Canada, J. Geophys. Res. Biogeosciences, 116, https://doi.org/10.1029/2010JG001512, 2011.

Alekseychik, P., Korrensalo, A., Mammarella, I., Launiainen, S., Tuittila, E.-S., Korpela, I., and Vesala, T.: Carbon balance of a Finnish bog: temporal variability and limiting factors based on 6 years of eddy-covariance data, Biogeosciences, 18, 4681–4704, https://doi.org/10.5194/bg-18-4681-2021, 2021.

Aslan-Sungur, G., Lee, X., Evrendilek, F., and Karakaya, N.: Large interannual variability in net ecosystem carbon dioxide exchange of a disturbed temperate peatland, Sci. Total Environ., 554–555, 192–202, https://doi.org/10.1016/j.scitotenv.2016.02.153, 2016.

Aurela, M., Riutta, T., Laurila, T., Tuovinen, J.-P., Vesala, T., Tuittila, E.-S., Rinne, J., Haapanala, S., and Laine, J.: CO2 exchange of a sedge fen in southern Finland—the impact of a drought period, Tellus B Chem. Phys. Meteorol., 59, 2007.

Bao, X., Li, Z., and Xie, F.: Environmental influences on light response parameters of net carbon exchange in two rotation croplands on the North China Plain, Sci. Rep., 9, 18702, https://doi.org/10.1038/s41598-019-55340-2, 2019.

Barichivich, J., Briffa, K. R., Myneni, R. B., Osborn, T. J., Melvin, T. M., Ciais, P., Piao, S., and Tucker, C.: Large-scale variations in the vegetation growing season and annual cycle of atmospheric CO2 at high northern latitudes from 1950 to 2011, Glob. Change Biol., 19, 3167–3183, https://doi.org/10.1111/gcb.12283, 2013.

van den Berg, M., van den Elzen, E., Ingwersen, J., Kosten, S., Lamers, L. P. M., and Streck, T.: Contribution of plant-induced pressurized flow to CH4 emission from a Phragmites fen, Sci. Rep., 10, 12304, https://doi.org/10.1038/s41598-020-69034-7, 2020.

Blodau, C.: Thermodynamic Control on Terminal Electron Transfer and Methanogenesis, in: ACS Symposium Series, vol. 1071, edited by: Tratnyek, P. G., Grundl, T. J., and Haderlein, S. B., American Chemical Society, Washington, DC, 65–83, https://doi.org/10.1021/bk-2011-1071.ch004, 2011.

Bubier, J. L., Crill, P. M., Moore, T. R., Savage, K., and Varner, R. K.: Seasonal patterns and controls on net ecosystem CO2 exchange in a boreal peatland complex, Glob. Biogeochem. Cycles, 12, 703–714, https://doi.org/10.1029/98GB02426, 1998.

https://doi.org/10.5194/egusphere-2026-1496
Preprint. Discussion started: 20 March 2026

Buzacott, A. J. V., Kruijt, B., Bataille, L., van Giersbergen, Q., Heuts, T. S., Fritz, C., Nouta, R., Erkens, G., Boonman, J., van den Berg, M., van Huissteden, J., and van der Velde, Y.: Drivers and Annual Totals of Methane Emissions From Dutch Peatlands, Glob. Change Biol., 30, e17590, https://doi.org/10.1111/gcb.17590, 2024.

Cai, Y., Yu, X., Zou, Y., Ding, S., and Min, Y.: Shrubification of herbaceous peatlands modulates root exudates, increasing rhizosphere soil CO2 emissions while decreasing CH4 emissions, CATENA, 245, 108282, https://doi.org/10.1016/j.catena.2024.108282, 2024.

Calabrese, S., Garcia, A., Wilmoth, J. L., Zhang, X., and Porporato, A.: Critical inundation level for methane emissions from wetlands, Environ. Res. Lett., 16, 044038, https://doi.org/10.1088/1748-9326/abedea, 2021.

Chen, N., Zhang, Y., Yuan, F., Song, C., Xu, M., Wang, Q., Hao, G., Bao, T., Zuo, Y., Liu, J., Zhang, T., Song, Y., Sun, L., Guo, Y., Zhang, H., Ma, G., Du, Y., Xu, X., and Wang, X.: Warming-induced vapor pressure deficit suppression of vegetation growth diminished in northern peatlands, Nat. Commun., 14, 7885, https://doi.org/10.1038/s41467-023-42932-w, 2023.

Chen, T. and Guestrin, C.: XGBoost: A Scalable Tree Boosting System, in: Proceedings of the 22nd ACM SIGKDD International Conference on Knowledge Discovery and Data Mining, 785–794, https://doi.org/10.1145/2939672.2939785, 2016.

Chivers, M. R., Turetsky, M. R., Waddington, J. M., Harden, J. W., and McGuire, A. D.: Effects of Experimental Water Table and Temperature Manipulations on Ecosystem CO2 Fluxes in an Alaskan Rich Fen, Ecosystems, 12, 1329–1342, https://doi.org/10.1007/s10021-009-9292-y, 2009.

Denager, T., Christiansen, J. R., Schneider, R. J. M., Langen, P., Quistgaard, T., and Stisen, S.: Combined water table and temperature dynamics control CO2 emission estimates from drained peatlands under rewetting and climate change scenarios, Biogeosciences, 23, 441–462, https://doi.org/10.5194/bg-23-441-2026, 2026.

Drollinger, S., Maier, A., and Glatzel, S.: Interannual and seasonal variability in carbon dioxide and methane fluxes of a pine peat bog in the Eastern Alps, Austria, Agric. For. Meteorol., 275, 69–78, https://doi.org/10.1016/j.agrformet.2019.05.015, 2019.

Estop-Aragonés, C. and Blodau, C.: Effects of experimental drying intensity and duration on respiration and methane production recovery in fen peat incubations, Soil Biol. Biochem., 47, 1–9, https://doi.org/10.1016/j.soilbio.2011.12.008, 2012.

Evans, C. D., Peacock, M., Baird, A. J., Artz, R. R. E., Burden, A., Callaghan, N., Chapman, P. J., Cooper, H. M., Coyle, M., Craig, E., Cumming, A., Dixon, S., Gauci, V., Grayson, R. P., Helfter, C., Heppell, C. M., Holden, J., Jones, D. L., Kaduk, J., Levy, P., Matthews, R., McNamara, N. P., Misselbrook, T., Oakley, S., Page, S. E., Rayment, M., Ridley, L. M., Stanley, K. M., Williamson, J. L., Worrall, F., and Morrison, R.: Overriding water table control on managed peatland greenhouse gas emissions, Nature, 593, 548–552, https://doi.org/10.1038/s41586-021-03523-1, 2021.

Falge, E., Baldocchi, D., Olson, R., Anthoni, P., Aubinet, M., Bernhofer, C., Burba, G., Ceulemans, R., Clement, R., Dolman, H., Granier, A., Gross, P., Grünwald, T., Hollinger, D., Jensen, N.-O., Katul, G., Keronen, P., Kowalski, A., Lai, C.

https://doi.org/10.5194/egusphere-2026-1496
Preprint. Discussion started: 20 March 2026

T., Law, B. E., Meyers, T., Moncrieff, J., Moors, E., Munger, J. W., Pilegaard, K., Rannik, Ü., Rebmann, C., Suyker, A., Tenhunen, J., Tu, K., Verma, S., Vesala, T., Wilson, K., and Wofsy, S.: Gap filling strategies for defensible annual sums of net ecosystem exchange, Agric. For. Meteorol., 107, 43–69, https://doi.org/10.1016/S0168-1923(00)00225-2, 2001.

Fan, S.-M., Wofsy, S. C., Bakwin, P. S., Jacob, D. J., and Fitzjarrald, D. R.: Atmosphere-biosphere exchange of CO2 and O3 in the central Amazon Forest, J. Geophys. Res. Atmospheres, 95, 16851–16864, https://doi.org/10.1029/JD095iD10p16851, 1990.

Farrick, K. K. and Price, J. S.: Ericaceous shrubs on abandoned block-cut peatlands: implications for soil water availability and Sphagnum restoration, Ecohydrology, 2, 530–540, https://doi.org/10.1002/eco.77, 2009.

Finkelstein, P. L. and Sims, P. F.: Sampling error in eddy correlation flux measurements, J. Geophys. Res. Atmospheres, 106, 3503–3509, https://doi.org/10.1029/2000JD900731, 2001.

Foken, T.: The Energy Balance Closure Problem: An Overview, Ecol. Appl., 18, 1351–1367, https://doi.org/10.1890/06-0922.1, 2008.

Frank, S., Dettmann, U., Piayda, A., Seidel, R., Amiri, E., Bamberger, S., Heidkamp, A., Heller, S., Holzträger, S., Kuwert, M., Lakeberg, S., Laqua, S., Minke, M., Nagel, S., Oehmke, W., Schemschat, B., Simon, C., Wittnebel, M., Wywias, H., and Tiemeyer, B.: Bericht zum Aufbau eines deutschlandweiten Moorbodenmonitorings für den Klimaschutz, Johann Heinrich von Thünen Institut, DE, 186 pp., https://doi.org/10.3220/253-2025-181, 2025.

Fratini, G., Ibrom, A., Arriga, N., Burba, G., and Papale, D.: Relative humidity effects on water vapour fluxes measured with closed-path eddy-covariance systems with short sampling lines, Agric. For. Meteorol., 165, 53–63, https://doi.org/10.1016/j.agrformet.2012.05.018, 2012.

Frolking, S., Talbot, J., Jones, M. C., Treat, C. C., Kauffman, J. B., Tuittila, E.-S., and Roulet, N.: Peatlands in the Earth's 21st century climate system, Environ. Rev., 19, 371–396, https://doi.org/10.1139/a11-014, 2011.

Gao, C., Sander, M., Agethen, S., and Knorr, K.-H.: Electron accepting capacity of dissolved and particulate organic matter control CO2 and CH4 formation in peat soils, Geochim. Cosmochim. Acta, 245, 266–277, https://doi.org/10.1016/j.gca.2018.11.004, 2019.

Gharun, M. and Behrens, N.: ETC L2 Fluxes from Amtsvenn, 2022-12-31–2024-12-31, 2025.

Gobin, R., Korboulewsky, N., Dumas, Y., and Balandier, P.: Transpiration of four common understorey plant species according to drought intensity in temperate forests, Ann. For. Sci., 72, https://doi.org/10.1007/s13595-015-0510-9, 2015.

Goodrich, J. P., Campbell, D. I., Clearwater, M. J., Rutledge, S., and Schipper, L. A.: High vapor pressure deficit constrains GPP and the light response of NEE at a Southern Hemisphere bog, Agric. For. Meteorol., 203, 54–63, https://doi.org/10.1016/j.agrformet.2015.01.001, 2015.

Grossiord, C., Buckley, T. N., Cernusak, L. A., Novick, K. A., Poulter, B., Siegwolf, R. T. W., Sperry, J. S., and McDowell, N. G.: Plant responses to rising vapor pressure deficit, New Phytol., 226, 1550–1566, https://doi.org/10.1111/nph.16485, 2020.

https://doi.org/10.5194/egusphere-2026-1496
Preprint. Discussion started: 20 March 2026

Guo, H., Cui, S., Nielsen, C. K., Tang, L., Pugliese, L., and Wu, S.: Harnessing the Low-Hanging Fruits: Rewetting Unmanaged Marginal Organic Soils to Achieve Maximal Greenhouse Gas Reduction, Environ. Sci. Technol., 59, 6521–6533, https://doi.org/10.1021/acs.est.4c12572, 2025.

Gyimah, A., Wu, J., Scott, R., and Gong, Y.: Agricultural drainage increases the photosynthetic capacity of boreal peatlands, Agric. Ecosyst. Environ., 300, 106984, https://doi.org/10.1016/j.agee.2020.106984, 2020.

Hamamoto, S., Dissanayaka, S. H., Kawamoto, K., Nagata, O., Komtatsu, T., and Moldrup, P.: Transport properties and pore-network structure in variably-saturated Sphagnum peat soil, Eur. J. Soil Sci., 67, 121–131, https://doi.org/10.1111/ejss.12312, 2016.

Hanson, P. J., Griffiths, N. A., Iversen, C. M., Norby, R. J., Sebestyen, S. D., Phillips, J. R., Chanton, J. P., Kolka, R. K., Malhotra, A., Oleheiser, K. C., Warren, J. M., Shi, X., Yang, X., Mao, J., and Ricciuto, D. M.: Rapid Net Carbon Loss From a Whole-Ecosystem Warmed Peatland, AGU Adv., 1, e2020AV000163, https://doi.org/10.1029/2020AV000163, 2020.

He, H. and Roulet, N. T.: Improved estimates of carbon dioxide emissions from drained peatlands support a reduction in emission factor, Commun. Earth Environ., 4, 436, https://doi.org/10.1038/s43247-023-01091-y, 2023.

He, K., Zhang, X., Ren, S., and Sun, J.: Delving Deep into Rectifiers: Surpassing Human-Level Performance on ImageNet Classification, in: 2015 IEEE International Conference on Computer Vision (ICCV), 1026–1034, https://doi.org/10.1109/ICCV.2015.123, 2015.

Heiskanen, L., Tuovinen, J.-P., Räsänen, A., Virtanen, T., Juutinen, S., Lohila, A., Penttilä, T., Linkosalmi, M., Mikola, J., Laurila, T., and Aurela, M.: Carbon dioxide and methane exchange of a patterned subarctic fen during two contrasting growing seasons, Biogeosciences, 18, 873–896, https://doi.org/10.5194/bg-18-873-2021, 2021.

Helbig, M., Živković, T., Alekseychik, P., Aurela, M., El-Madany, T. S., Euskirchen, E. S., Flanagan, L. B., Griffis, T. J., Hanson, P. J., Hattakka, J., Helfter, C., Hirano, T., Humphreys, E. R., Kiely, G., Kolka, R. K., Laurila, T., Leahy, P. G., Lohila, A., Mammarella, I., Nilsson, M. B., Panov, A., Parmentier, F. J. W., Peichl, M., Rinne, J., Roman, D. T., Sonnentag, O., Tuittila, E.-S., Ueyama, M., Vesala, T., Vestin, P., Weldon, S., Weslien, P., and Zaehle, S.: Warming response of peatland CO2 sink is sensitive to seasonality in warming trends, Nat. Clim. Change, 12, 743–749, https://doi.org/10.1038/s41558-022-01428-z, 2022.

Helfter, C., Campbell, C., Dinsmore, K. J., Drewer, J., Coyle, M., Anderson, M., Skiba, U., Nemitz, E., Billett, M. F., and Sutton, M. A.: Drivers of long-term variability in CO2 net ecosystem exchange in a temperate peatland, Biogeosciences, 12, 1799–1811, https://doi.org/10.5194/bg-12-1799-2015, 2015.

Hollinger, D. Y. and Richardson, A. D.: Uncertainty in eddy covariance measurements and its application to physiological models, Tree Physiol., 25, 873–885, https://doi.org/10.1093/treephys/25.7.873, 2005.

Huang, M., Piao, S., Ciais, P., Peñuelas, J., Wang, X., Keenan, T. F., Peng, S., Berry, J. A., Wang, K., Mao, J., Alkama, R., Cescatti, A., Cuntz, M., De Deurwaerder, H., Gao, M., He, Y., Liu, Y., Luo, Y., Myneni, R. B., Niu, S., Shi, X., Yuan, W., Verbeeck, H., Wang, T., Wu, J., and Janssens, I. A.: Air temperature optima of vegetation productivity across global biomes, Nat. Ecol. Evol., 3, 772–779, https://doi.org/10.1038/s41559-019-0838-x, 2019.

https://doi.org/10.5194/egusphere-2026-1496
Preprint. Discussion started: 20 March 2026

Humphreys, E. R., Lafleur, P. M., Flanagan, L. B., Hedstrom, N., Syed, K. H., Glenn, A. J., and Granger, R.: Summer carbon dioxide and water vapor fluxes across a range of northern peatlands, J. Geophys. Res. Biogeosciences, 111, https://doi.org/10.1029/2005JG000111, 2006.

Humphreys, E. R., Charron, C., Brown, M., and Jones, R.: Two Bogs in the Canadian Hudson Bay Lowlands and a Temperate Bog Reveal Similar Annual Net Ecosystem Exchange of CO2, Arct. Antarct. Alp. Res., 46, 103–113, https://doi.org/10.1657/1938-4246.46.1.103, 2014.

Hurkuck, M., Brümmer, C., and Kutsch, W. L.: Near-neutral carbon dioxide balance at a seminatural, temperate bog ecosystem, J. Geophys. Res. Biogeosciences, 121, 370–384, https://doi.org/10.1002/2015JG003195, 2016.

Intergovernmental Panel on Climate Change (IPCC): Climate Change 2022 – Impacts, Adaptation and Vulnerability: Working Group II Contribution to the Sixth Assessment Report of the Intergovernmental Panel on Climate Change, Cambridge University Press, Cambridge, https://doi.org/10.1017/9781009325844, 2023.

IPCC: 2013 Supplement to the 2006 IPCC Guidelines for National Greenhouse Gas Inventories: Wetlands, edited by: Hiraishi, T., Krug, T., Tanabe, K., Srivastava, N., Baasansuren, J., Fukuda, M., and Troxler, T. G., IPCC, Switzerland, 2014.

Järveoja, J., Nilsson, M. B., Gažovič, M., Crill, P. M., and Peichl, M.: Partitioning of the net CO2 exchange using an automated chamber system reveals plant phenology as key control of production and respiration fluxes in a boreal peatland, Glob. Change Biol., 24, 3436–3451, https://doi.org/10.1111/gcb.14292, 2018.

Juszczak, R., Humphreys, E., Acosta, M., Michalak-Galczewska, M., Kayzer, D., and Olejnik, J.: Ecosystem respiration in a heterogeneous temperate peatland and its sensitivity to peat temperature and water table depth, Plant Soil, 366, 505–520, https://doi.org/10.1007/s11104-012-1441-y, 2013.

Kalhori, A., Wille, C., Gottschalk, P., Li, Z., Hashemi, J., Kemper, K., and Sachs, T.: Temporally dynamic carbon dioxide and methane emission factors for rewetted peatlands, Commun. Earth Environ., 5, 1–11, https://doi.org/10.1038/s43247-024-01226-9, 2024.

Kingma, D. and Ba, J.: Adam: A Method for Stochastic Optimization, Int. Conf. Learn. Represent., 2014.

Kljun, N., Calanca, P., Rotach, M. W., and Schmid, H. P.: A simple two-dimensional parameterisation for Flux Footprint Prediction (FFP), Geosci. Model Dev., 8, 3695–3713, https://doi.org/10.5194/gmd-8-3695-2015, 2015.

Knorr, K.-H., Lischeid, G., and Blodau, C.: Dynamics of redox processes in a minerotrophic fen exposed to a water table manipulation, Geoderma, 153, 379–392, https://doi.org/10.1016/j.geoderma.2009.08.023, 2009.

Koch, J., Elsgaard, L., Greve, M. H., Gyldenkærne, S., Hermansen, C., Levin, G., Wu, S., and Stisen, S.: Water-table-driven greenhouse gas emission estimates guide peatland restoration at national scale, Biogeosciences, 20, 2387–2403, https://doi.org/10.5194/bg-20-2387-2023, 2023.

Korrensalo, A., Mehtätalo, L., Alekseychik, P., Uljas, S., Mammarella, I., Vesala, T., and Tuittila, E.-S.: Varying Vegetation Composition, Respiration and Photosynthesis Decrease Temporal Variability of the CO2 Sink in a Boreal Bog, Ecosystems, 23, 842–858, https://doi.org/10.1007/s10021-019-00434-1, 2020.

https://doi.org/10.5194/egusphere-2026-1496
Preprint. Discussion started: 20 March 2026

Kross, A., Seaquist, J. W., and Roulet, N. T.: Light use efficiency of peatlands: Variability and suitability for modeling ecosystem production, Remote Sens. Environ., 183, 239–249, https://doi.org/10.1016/j.rse.2016.05.004, 2016.

Lafleur, P. M., Hember, R. A., Admiral, S. W., and Roulet, N. T.: Annual and seasonal variability in evapotranspiration and water table at a shrub-covered bog in southern Ontario, Canada, Hydrol. Process., 19, 3533–3550, https://doi.org/10.1002/hyp.5842, 2005a.

Lafleur, P. M., Moore, T. R., Roulet, N. T., and Frolking, S.: Ecosystem Respiration in a Cool Temperate Bog Depends on Peat Temperature But Not Water Table, Ecosystems, 8, 619–629, https://doi.org/10.1007/s10021-003-0131-2, 2005b.

Laine, A. M., Mäkiranta, P., Laiho, R., Mehtätalo, L., Penttilä, T., Korrensalo, A., Minkkinen, K., Fritze, H., and Tuittila, E.-S.: Warming impacts on boreal fen CO2 exchange under wet and dry conditions, Glob. Change Biol., 25, 1995–2008, https://doi.org/10.1111/gcb.14617, 2019.

Lakshminarayanan, B., Pritzel, A., and Blundell, C.: Simple and Scalable Predictive Uncertainty Estimation using Deep Ensembles, in: Advances in Neural Information Processing Systems, 2017.

Lemmens, M., Teickner, H., Lamentowicz, M., Thomas, C. L., Glatzel, S., Gałka, M., Draga, M., and Knorr, K.-H.: Multi-proxy high-resolution geochemical analysis reveals ecological baselines and evaluates potential restoration trajectories in European ombrotrophic peatlands, Ecol. Indic., 183, 114648, https://doi.org/10.1016/j.ecolind.2026.114648, 2026.

Li, C., Zhang, D., Zhang, S., Wen, Y., Wang, W., Chen, Y., and Peng, J.: Atmospheric Vapor Pressure Deficit Outweighs Soil Moisture Deficit in Controlling Global Ecosystem Water Use Efficiency, J. Geophys. Res. Biogeosciences, 130, e2024JG008605, https://doi.org/10.1029/2024JG008605, 2025.

Li, Q., Gogo, S., Leroy, F., Guimbaud, C., and Laggoun-Défarge, F.: Response of Peatland CO2 and CH4 Fluxes to Experimental Warming and the Carbon Balance, Front. Earth Sci., 9, https://doi.org/10.3389/feart.2021.631368, 2021.

Limpens, J., Berendse, F., Blodau, C., Canadell, J. G., Freeman, C., Holden, J., Roulet, N., Rydin, H., and Schaepman-Strub, G.: Peatlands and the carbon cycle: from local processes to global implications – a synthesis, Biogeosciences, 5, 1475–1491, https://doi.org/10.5194/bg-5-1475-2008, 2008.

Liu, H., Rezanezhad, F., Zhao, Y., He, H., Van Cappellen, P., and Lennartz, B.: The apparent temperature sensitivity (Q10) of peat soil respiration: A synthesis study, Geoderma, 443, 116844, https://doi.org/10.1016/j.geoderma.2024.116844, 2024.

Lloyd, J. and Taylor, J. A.: On the Temperature Dependence of Soil Respiration, Funct. Ecol., 8, 315–323, https://doi.org/10.2307/2389824, 1994.

Lund, M., Lafleur, P. M., Roulet, N. T., Lindroth, A., Christensen, T. R., Aurela, M., Chojnicki, B. H., Flanagan, L. B., Humphreys, E. R., Laurila, T., Oechel, W. C., Olejnik, J., Rinne, J., Schubert, P., and Nilsson, M. B.: Variability in exchange of CO2 across 12 northern peatland and tundra sites, Glob. Change Biol., 16, 2436–2448, https://doi.org/10.1111/j.1365-2486.2009.02104.x, 2010.

Ma, L., Zhu, G., Chen, B., Zhang, K., Niu, S., Wang, J., Ciais, P., and Zuo, H.: A globally robust relationship between water table decline, subsidence rate, and carbon release from peatlands, Commun. Earth Environ., 3, 1–14, https://doi.org/10.1038/s43247-022-00590-8, 2022.

https://doi.org/10.5194/egusphere-2026-1496
Preprint. Discussion started: 20 March 2026

Mäkiranta, P., Laiho, R., Fritze, H., Hytönen, J., Laine, J., and Minkkinen, K.: Indirect regulation of heterotrophic peat soil respiration by water level via microbial community structure and temperature sensitivity, Soil Biol. Biochem., 41, 695–703, https://doi.org/10.1016/j.soilbio.2009.01.004, 2009.

Massmann, A., Gentine, P., and Lin, C.: When Does Vapor Pressure Deficit Drive or Reduce Evapotranspiration?, J. Adv. Model. Earth Syst., 11, 3305–3320, https://doi.org/10.1029/2019MS001790, 2019.

Mauder, M. and Foken, T.: Documentation and instruction manual of the eddy-covariance software package TK3, 2011.

Mauder, M., Jung, M., Stoy, P., Nelson, J., and Wanner, L.: Energy balance closure at FLUXNET sites revisited, Agric. For. Meteorol., 358, 110235, https://doi.org/10.1016/j.agrformet.2024.110235, 2024.

Michaletz, S. T., Weiser, M. D., McDowell, N. G., Zhou, J., Kaspari, M., Helliker, B. R., and Enquist, B. J.: The energetic and carbon economic origins of leaf thermoregulation, Nat. Plants, 2, 16129, https://doi.org/10.1038/nplants.2016.129, 2016.

Moncrieff, J., Clement, R., Finnigan, J., and Meyers, T.: Averaging, Detrending, and Filtering of Eddy Covariance Time Series, in: Handbook of Micrometeorology: A Guide for Surface Flux Measurement and Analysis, edited by: Lee, X., Massman, W., and Law, B., Springer Netherlands, Dordrecht, 7–31, https://doi.org/10.1007/1-4020-2265-4_2, 2005.

Munir, T. M., Perkins, M., Kaing, E., and Strack, M.: Carbon dioxide flux and net primary production of a boreal treed bog: Responses to warming and water-table-lowering simulations of climate change, Biogeosciences, 12, 1091–1111, https://doi.org/10.5194/bg-12-1091-2015, 2015.

Muñoz-Sabater, J., Dutra, E., Agustí-Panareda, A., Albergel, C., Arduini, G., Balsamo, G., Boussetta, S., Choulga, M., Harrigan, S., Hersbach, H., Martens, B., Miralles, D. G., Piles, M., Rodríguez-Fernández, N. J., Zsoter, E., Buontempo, C., and Thépaut, J.-N.: ERA5-Land: a state-of-the-art global reanalysis dataset for land applications, Earth Syst. Sci. Data, 13, 4349–4383, https://doi.org/10.5194/essd-13-4349-2021, 2021.

Nielsen, C. K., Elsgaard, L., Jørgensen, U., and Lærke, P. E.: Soil greenhouse gas emissions from drained and rewetted agricultural bare peat mesocosms are linked to geochemistry, Sci. Total Environ., 896, 165083, https://doi.org/10.1016/j.scitotenv.2023.165083, 2023.

Novick, K. A., Ficklin, D. L., Stoy, P. C., Williams, C. A., Bohrer, G., Oishi, A. C., Papuga, S. A., Blanken, P. D., Noormets, A., Sulman, B. N., Scott, R. L., Wang, L., and Phillips, R. P.: The increasing importance of atmospheric demand for ecosystem water and carbon fluxes, Nat. Clim. Change, 6, 1023–1027, https://doi.org/10.1038/nclimate3114, 2016.

Novick, K. A., Ficklin, D. L., Grossiord, C., Konings, A. G., Martínez-Vilalta, J., Sadok, W., Trugman, A. T., Williams, A. P., Wright, A. J., Abatzoglou, J. T., Dannenberg, M. P., Gentine, P., Guan, K., Johnston, M. R., Lowman, L. E. L., Moore, D. J. P., and McDowell, N. G.: The impacts of rising vapour pressure deficit in natural and managed ecosystems, Plant Cell Environ., 47, 3561–3589, https://doi.org/10.1111/pce.14846, 2024.

Nugent, K. A., Strachan, I. B., Strack, M., Roulet, N. T., and Rochefort, L.: Multi-year net ecosystem carbon balance of a restored peatland reveals a return to carbon sink, Glob. Change Biol., 24, 5751–5768, https://doi.org/10.1111/gcb.14449, 2018.

https://doi.org/10.5194/egusphere-2026-1496
Preprint. Discussion started: 20 March 2026

Oestmann, J., Dettmann, U., Düvel, D., and Tiemeyer, B.: Experimental warming increased greenhouse gas emissions of a near-natural peatland and Sphagnum farming sites, Plant Soil, 480, 85–104, https://doi.org/10.1007/s11104-022-05561-8, 2022.

Olson, D. M., Griffis, T. J., Noormets, A., Kolka, R., and Chen, J.: Interannual, seasonal, and retrospective analysis of the methane and carbon dioxide budgets of a temperate peatland, J. Geophys. Res. Biogeosciences, 118, 226–238, https://doi.org/10.1002/jgrg.20031, 2013.

Osonubi, O. and Davies, W. J.: The influence of plant water stress on stomatal control of gas exchange at different levels of atmospheric humidity, Oecologia, 46, 1–6, https://doi.org/10.1007/BF00346957, 1980.

Otieno, D., Lindner, S., Muhr, J., and Borken, W.: Sensitivity of Peatland Herbaceous Vegetation to Vapor Pressure Deficit Influences Net Ecosystem CO2 Exchange, Wetlands, 32, 895–905, https://doi.org/10.1007/s13157-012-0322-8, 2012.

Pastorello, G., Trotta, C., Canfora, E., Chu, H., Christianson, D., Cheah, Y.-W., Poindexter, C., Chen, J., Elbashandy, A., Humphrey, M., Isaac, P., Polidori, D., Reichstein, M., Ribeca, A., van Ingen, C., Vuichard, N., Zhang, L., Amiro, B., Ammann, C., Arain, M. A., Ardö, J., Arkebauer, T., Arndt, S. K., Arriga, N., Aubinet, M., Aurela, M., Baldocchi, D., Barr, A., Beamesderfer, E., Marchesini, L. B., Bergeron, O., Beringer, J., Bernhofer, C., Berveiller, D., Billesbach, D., Black, T. A., Blanken, P. D., Bohrer, G., Boike, J., Bolstad, P. V., Bonal, D., Bonnefond, J.-M., Bowling, D. R., Bracho, R., Brodeur, J., Brümmer, C., Buchmann, N., Burban, B., Burns, S. P., Buysse, P., Cale, P., Cavagna, M., Cellier, P., Chen, S., Chini, I., Christensen, T. R., Cleverly, J., Collalti, A., Consalvo, C., Cook, B. D., Cook, D., Coursolle, C., Cremonese, E., Curtis, P. S., D'Andrea, E., da Rocha, H., Dai, X., Davis, K. J., Cinti, B. D., Grandcourt, A. de, Ligne, A. D., De Oliveira, R. C., Delpierre, N., Desai, A. R., Di Bella, C. M., Tommasi, P. di, Dolman, H., Domingo, F., Dong, G., Dore, S., Duce, P., Dufrêne, E., Dunn, A., Dušek, J., Eamus, D., Eichelmann, U., ElKhidir, H. A. M., Eugster, W., Ewenz, C. M., Ewers, B., Famulari, D., Fares, S., Feigenwinter, I., Feitz, A., Fensholt, R., Filippa, G., Fischer, M., Frank, J., Galvagno, M., et al.: The FLUXNET2015 dataset and the ONEFlux processing pipeline for eddy covariance data, Sci. Data, 7, 225, https://doi.org/10.1038/s41597-020-0534-3, 2020.

Pedregosa, F., Varoquaux, G., Gramfort, A., Michel, V., Thirion, B., Grisel, O., Blondel, M., Prettenhofer, P., Weiss, R., Dubourg, V., Vanderplas, J., Passos, A., Cournapeau, D., Brucher, M., Perrot, M., and Duchesnay, E.: Scikit-learn: Machine Learning in Python, J. Mach. Learn. Res., 12, 2825–2830, 2011.

Peichl, M., Öquist, M., Ottosson Löfvenius, M., Ilstedt, U., Sagerfors, J., Grelle, A., Lindroth, A., and Nilsson, M. B.: A 12-year record reveals pre-growing season temperature and water table level threshold effects on the net carbon dioxide exchange in a boreal fen, Environ. Res. Lett., 9, 055006, https://doi.org/10.1088/1748-9326/9/5/055006, 2014.

Peichl, M., Gažovič, M., Vermeij, I., de Goede, E., Sonnentag, O., Limpens, J., and Nilsson, M. B.: Peatland vegetation composition and phenology drive the seasonal trajectory of maximum gross primary production, Sci. Rep., 8, 8012, https://doi.org/10.1038/s41598-018-26147-4, 2018.

Pinsonneault, A. J., Moore, T. R., and Roulet, N. T.: Effects of long-term fertilization on peat stoichiometry and associated microbial enzyme activity in an ombrotrophic bog, Biogeochemistry, 129, 149–164, 2016.

https://doi.org/10.5194/egusphere-2026-1496
Preprint. Discussion started: 20 March 2026

Poczta, P., Urbaniak, M., Sachs, T., Harenda, K. M., Klarzyńska, A., Juszczak, R., Schüttemeyer, D., Czernecki, B., Kryszak, A., and Chojnicki, B. H.: A multi-year study of ecosystem production and its relation to biophysical factors over a temperate peatland, Agric. For. Meteorol., 338, 109529, https://doi.org/10.1016/j.agrformet.2023.109529, 2023.

Qiu, C., Ciais, P., Zhu, D., Guenet, B., Chang, J., Chaudhary, N., Kleinen, T., Li, X., Müller, J., Xi, Y., Zhang, W., Ballantyne, A., Brewer, S. C., Brovkin, V., Charman, D. J., Gustafson, A., Gallego-Sala, A. V., Gasser, T., Holden, J., Joos, F., Kwon, M. J., Lauerwald, R., Miller, P. A., Peng, S., Page, S., Smith, B., Stocker, B. D., Sannel, A. B. K., Salmon, E., Schurgers, G., Shurpali, N. J., Wårlind, D., and Westermann, S.: A strong mitigation scenario maintains climate neutrality of northern peatlands, One Earth, 5, 86–97, https://doi.org/10.1016/j.oneear.2021.12.008, 2022.

Quin, S. L. O., Artz, R. R. E., Coupar, A. M., and Woodin, S. J.: Calluna vulgaris-dominated upland heathland sequesters more CO2 annually than grass-dominated upland heathland, Sci. Total Environ., 505, 740–747, https://doi.org/10.1016/j.scitotenv.2014.10.037, 2015.

Rankin, T., Roulet, N. T., and Moore, T. R.: Controls on autotrophic and heterotrophic respiration in an ombrotrophic bog, Biogeosciences, 19, 3285–3303, https://doi.org/10.5194/bg-19-3285-2022, 2022.

Rankin, T., Roulet, N., Humphreys, E., Peichl, M., and Järveoja, J.: Partitioning autotrophic and heterotrophic respiration in an ombrotrophic bog, Front. Earth Sci., 11, https://doi.org/10.3389/feart.2023.1263418, 2023.

Reichstein, M., Falge, E., Baldocchi, D., Papale, D., Aubinet, M., Berbigier, P., Bernhofer, C., Buchmann, N., Gilmanov, T., Granier, A., Grunwald, T., Havrankova, K., Ilvesniemi, H., Janous, D., Knohl, A., Laurila, T., Lohila, A., Loustau, D., Matteucci, G., Meyers, T., Miglietta, F., Ourcival, J.-M., Pumpanen, J., Rambal, S., Rotenberg, E., Sanz, M., Tenhunen, J., Seufert, G., Vaccari, F., Vesala, T., Yakir, D., and Valentini, R.: On the separation of net ecosystem exchange into assimilation and ecosystem respiration: review and improved algorithm, Glob. Change Biol., 11, 1424–1439, https://doi.org/10.1111/j.1365-2486.2005.001002.x, 2005.

Sabbatini, S., Mammarella, I., Arriga, N., Fratini, G., Graf, A., Hörtnagl, L., Ibrom, A., Longdoz, B., Mauder, M., Merbold, L., Metzger, S., Montagnani, L., Pitacco, A., Rebmann, C., Sedlák, P., Šigut, L., Vitale, D., and Papale, D.: Eddy covariance raw data processing for CO2 and energy fluxes calculation at ICOS ecosystem stations, Int. Agrophysics, 32, 495–515, https://doi.org/10.1515/intag-2017-0043, 2018.

Satriawan, T. W., Nyberg, M., Lee, S.-C., Christen, A., Black, T. A., Johnson, M. S., Nesic, Z., Merkens, M., and Knox, S. H.: Interannual variability of carbon dioxide (CO2) and methane (CH4) fluxes in a rewetted temperate bog, Agric. For. Meteorol., 342, 109696, https://doi.org/10.1016/j.agrformet.2023.109696, 2023.

Seabold, S. and Perktold, J.: statsmodels: Econometric and statistical modeling with python, in: 9th Python in Science Conference, 2010.

Shekhar, A., Buchmann, N., Humphrey, V., and Gharun, M.: More than three-fold increase in compound soil and air dryness across Europe by the end of 21st century, Weather Clim. Extrem., 44, 100666, https://doi.org/10.1016/j.wace.2024.100666, 2024.

https://doi.org/10.5194/egusphere-2026-1496
Preprint. Discussion started: 20 March 2026

Speranskaya, L., Campbell, D. I., Lafleur, P. M., and Humphreys, E. R.: Peatland evaporation across hemispheres: contrasting controls and sensitivity to climate warming driven by plant functional types, Biogeosciences, 21, 1173–1190, https://doi.org/10.5194/bg-21-1173-2024, 2024.

Swails, E. E., Ardón, M., Krauss, K. W., Peralta, A. L., Emanuel, R. E., Helton, A. M., Morse, J. L., Gutenberg, L., Cormier, N., Shoch, D., Settlemyer, S., Soderholm, E., Boutin, B. P., Peoples, C., and Ward, S.: Response of soil respiration to changes in soil temperature and water table level in drained and restored peatlands of the southeastern United States, Carbon Balance Manag., 17, 18, https://doi.org/10.1186/s13021-022-00219-5, 2022.

Tiemeyer, B., Albiac Borraz, E., Augustin, J., Bechtold, M., Beetz, S., Beyer, C., Drösler, M., Ebli, M., Eickenscheidt, T., Fiedler, S., Förster, C., Freibauer, A., Giebels, M., Glatzel, S., Heinichen, J., Hoffmann, M., Höper, H., Jurasinski, G., Leiber-Sauheitl, K., Peichl-Brak, M., Roßkopf, N., Sommer, M., and Zeitz, J.: High emissions of greenhouse gases from grasslands on peat and other organic soils, Glob. Change Biol., 22, 4134–4149, https://doi.org/10.1111/gcb.13303, 2016.

Tiemeyer, B., Freibauer, A., Borraz, E. A., Augustin, J., Bechtold, M., Beetz, S., Beyer, C., Ebli, M., Eickenscheidt, T., Fiedler, S., Förster, C., Gensior, A., Giebels, M., Glatzel, S., Heinichen, J., Hoffmann, M., Höper, H., Jurasinski, G., Laggner, A., Leiber-Sauheitl, K., Peichl-Brak, M., and Drösler, M.: A new methodology for organic soils in national greenhouse gas inventories: Data synthesis, derivation and application, Ecol. Indic., 109, 105838, https://doi.org/10.1016/j.ecolind.2019.105838, 2020.

Ueyama, M., Iwata, H., and Harazono, Y.: Autumn warming reduces the CO2 sink of a black spruce forest in interior Alaska based on a nine-year eddy covariance measurement, Glob. Change Biol., 20, 1161–1173, https://doi.org/10.1111/gcb.12434, 2014.

Umweltbundesamt: Submission under the United Nations Framework Convention on Climate Change and the Kyoto Protocol 2022, Umweltbundesamt, 2022.

Vekuri, H., Tuovinen, J.-P., Kulmala, L., Aurela, M., Thum, T., Liski, J., and Lohila, A.: Improved uncertainty estimates for eddy covariance-based carbon dioxide balances using deep ensembles for gap-filling, Agric. For. Meteorol., 371, 110558, https://doi.org/10.1016/j.agrformet.2025.110558, 2025.

Vickers, D. and Mahrt, L.: Quality Control and Flux Sampling Problems for Tower and Aircraft Data, J. Atmospheric Ocean. Technol., 14, 512–526, https://doi.org/10.1175/1520-0426(1997)014%3C0512:QCAFSP%3E2.0.CO;2, 1997.

Voigt, C., Lamprecht, R. E., Marushchak, M. E., Lind, S. E., Novakovskiy, A., Aurela, M., Martikainen, P. J., and Biasi, C.: Warming of subarctic tundra increases emissions of all three important greenhouse gases – carbon dioxide, methane, and nitrous oxide, Glob. Change Biol., 23, 3121–3138, https://doi.org/10.1111/gcb.13563, 2017.

de Vries, F. T. and Caruso, T.: Eating from the same plate? Revisiting the role of labile carbon inputs in the soil food web, Soil Biol. Biochem., 102, 4–9, https://doi.org/10.1016/j.soilbio.2016.06.023, 2016.

Waddington, J. M., Rotenberg, P. A., and Warren, F. J.: Peat CO2 production in a natural and cutover peatland: Implications for restoration, Biogeochemistry, 54, 115–130, https://doi.org/10.1023/A:1010617207537, 2001.

https://doi.org/10.5194/egusphere-2026-1496
Preprint. Discussion started: 20 March 2026

Walker, T. N., Ward, S. E., Ostle, N. J., and Bardgett, R. D.: Contrasting growth responses of dominant peatland plants to warming and vegetation composition, Oecologia, 178, 141–151, https://doi.org/10.1007/s00442-015-3254-1, 2015.

Wang, H., Yan, S., Ciais, P., Wigneron, J.-P., Liu, L., Li, Y., Fu, Z., Ma, H., Liang, Z., Wei, F., Wang, Y., and Li, S.: Exploring complex water stress-gross primary production relationships: Impact of climatic drivers, main effects, and interactive effects, Glob. Change Biol., 28, 4110–4123, https://doi.org/10.1111/gcb.16201, 2022.

Ward, S. E., Ostle, N. J., Oakley, S., Quirk, H., Henrys, P. A., and Bardgett, R. D.: Warming effects on greenhouse gas fluxes in peatlands are modulated by vegetation composition, Ecol. Lett., 16, 1285–1293, https://doi.org/10.1111/ele.12167, 2013.

Waring, R. H., Landsberg, J. J., and Williams, M.: Net primary production of forests: a constant fraction of gross primary production?, Tree Physiol., 18, 129–134, https://doi.org/10.1093/treephys/18.2.129, 1998.

Webb, E. K., Pearman, G. I., and Leuning, R.: Correction of flux measurements for density effects due to heat and water vapour transfer, Q. J. R. Meteorol. Soc., 106, 85–100, https://doi.org/10.1002/qj.49710644707, 1980.

Wilczak, J. M., Oncley, S. P., and Stage, S. A.: Sonic Anemometer Tilt Correction Algorithms, Bound.-Layer Meteorol., 99, 127–150, https://doi.org/10.1023/A:1018966204465, 2001.

Wilson, D., Farrell, C. A., Fallon, D., Moser, G., Müller, C., and Renou-Wilson, F.: Multiyear greenhouse gas balances at a rewetted temperate peatland, Glob. Change Biol., 22, 4080–4095, https://doi.org/10.1111/gcb.13325, 2016.

Wutzler, T., Lucas-Moffat, A., Migliavacca, M., Knauer, J., Sickel, K., Šigut, L., Menzer, O., and Reichstein, M.: Basic and extensible post-processing of eddy covariance flux data with REddyProc, Biogeosciences, 15, 5015–5030, https://doi.org/10.5194/bg-15-5015-2018, 2018.

Yu, Z., Loisel, J., Brosseau, D. P., Beilman, D. W., and Hunt, S. J.: Global peatland dynamics since the Last Glacial Maximum, Geophys. Res. Lett., 37, L13402, https://doi.org/10.1029/2010GL043584, 2010.

Zhang, W., Hu, Z., Audet, J., Davidson, T. A., Kang, E., Kang, X., Li, Y., Zhang, X., and Wang, J.: Effects of water table level and nitrogen deposition on methane and nitrous oxide emissions in an alpine peatland, Biogeosciences, 19, 5187–5197, https://doi.org/10.5194/bg-19-5187-2022, 2022.

Zhang, X., Friedl, M. A., Schaaf, C. B., Strahler, A. H., Hodges, J. C. F., Gao, F., Reed, B. C., and Huete, A.: Monitoring vegetation phenology using MODIS, Remote Sens. Environ., 84, 471–475, https://doi.org/10.1016/S0034-4257(02)00135-9, 2003.

Zhao, Y., Feng, X., Pihlatie, M., Putkinen, A., Männikkö, M., Wang, H., Liu, C., Aurela, M., and Li, X.: Warming enhances soil carbon accumulation in boreal Sphagnum peatlands, Nat. Ecol. Evol., https://doi.org/10.1038/s41559-026-02982-x, 2026.